RSC Advances

REVIEW

View Article Online
View Journal | View Issue

Cite this: *RSC Adv.*, 2025, **15**, 50692

Phthalocyanine-based covalent organic frameworks: bridging molecular design and catalytic performance in CO_2 reduction

Yingying Li,* Haiyan Song, Wenbo Zhu, Wenduo Li and Chao Shuai

Covalent organic frameworks (COFs) are a type of porous material composed entirely of organic substances, featuring highly ordered structure, tunable pores, and customizable functions. They perfectly integrate the diversity and variability of organic materials with the characteristics of porous materials, and have shown great application prospects in numerous fields, such as energy, environment, catalysis, sensing, biomedicine. As an emerging high-performance material, the basic research and application exploration of COFs are currently in a stage of vigorous development, and it is also a popular frontier field in interdisciplinary research. Recently, due to the unique properties of the phthalocyanine units, phthalocyanine-based covalent organic framework materials (Pc-COFs) have attracted extensive attention and developed rapidly. This paper systematically reviews the research progress of Pc-COFs materials. Firstly, a detailed analysis was conducted on the design and synthesis techniques of Pc-COFs, summarizing the topological types, building units and linker types of Pc-COFs that have been reported. Then, the latest application progress of Pc-COFs in the field of carbon dioxide reduction was deeply explored, listing the catalytic effects of different configuration Pc-COFs catalysts in electrocatalytic and photocatalytic reactions. Finally, the existing challenges and future development prospects of Pc-COFscatalysts were reviewed and outlined.

Received 26th August 2025
Accepted 29th November 2025

DOI: 10.1039/d5ra06357d

rsc.li/rsc-advances

1. Introduction

Phthalocyanine is a large-ring compound with a structure similar to that of porphyrin, but it is entirely synthetic. Phthalocyanine ring has a cavity that can hold metal ions or non-metallic elements to form a variety of metal phthalocyanines or non-metallic phthalocyanine compounds (Fig. 1). This structural diversity enables phthalocyanine compounds to have a wide range of properties and applications. Besides being used as pigments and dyes, they are also employed in chemical sensors, electroluminescent devices, liquid crystal display materials, solar cell materials fields.[1–5] Additionally, phthalocyanines can also serve as catalysts to facilitate various chemical reactions with the advantages of mild reaction conditions and high efficiency.[6–10]

The unique properties of phthalocyanines have driven rapid progress in their application as building units for COFs in recent years,[11] providing new insights for the development of novel functional materials. Owing to their excellent optical, electrical, magnetic properties, Pc-COFs exhibit a broad range of applications in catalysis, sensing, separation, and related fields.[12–15] Additionally, research on Pc-COFs also encompasses the composite and modification with other materials. By forming composites with metal nanoparticles, polymers, and functional materials, the application scope and performance of Pc-COFs can be further expanded.[16–18] Given the rapid development and growing interest in Pc-COFs, several review articles in this field have been published during the past several years. In 2021, Chen *et al.* reviewed the progress achieved in the design, synthesis and application of porphyrin- and porphyrinoid-based covalent organic frameworks, highlighting their applications in gas absorption, storage of energy, optoelectronics, and catalysis.[19] In 2022, Huang *et al.* systematically summarized the electrocatalytic applications of Por- and Pc-based COFs. Their work covered four critical reactions: CO_2 reduction (CO_2RR), hydrogen evolution (HER), along with oxygen evolution and reduction (OER and ORR).[20] More recently, Kharissova *et al.* discussed the potential of using porphyrins, phthalocyanines, related macrocycles, and their

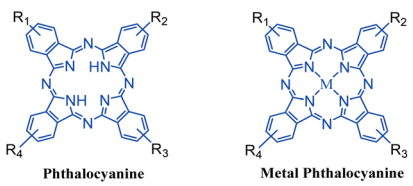

Fig. 1 Structure of phthalocyanine and metal phthalocyanine.

Gansu Key Laboratory of Efficient Utilization of Oil and Gas Resources in Longdong, College of Petroleum and Chemical Engineering, Longdong University, Qingyang, 745000, P. R. China. E-mail: liyingyinghx@163.com

metal complexes in photochemical and electrochemical water splitting.[21] In light of the ongoing research progress, a timely review of recent achievements is highly warranted. Moreover, the existing literature primarily focuses on porphyrin-based COFs and offers limited discussion on Pc-COFs. Given this gap, a comprehensive review dedicated to the research progress of Pc-COFs materials is of particular significance.

Herein, we aim to review the advances in the design, synthesis and application of Pc-COFs. This article begins by examining the rational design and selection of building units and linkers for constructing Pc-COFs with diverse topologies. Subsequently, it summarizes the synthesis methods of Pc-COFs and discusses their applications, with a particular focus on electrocatalytic and photocatalytic carbon dioxide reduction. Finally, the challenges and future opportunities in the development of Pc-COFs are highlighted.

2. Design of phthalocyanine based COFs

Owing to the rigid planar structure of phthalocyanine, the synthesis strategies of [4 + 2] and [4 + 4] are usually employed to assemble Pc-COFs. Here, the [4 + 2] and [4 + 4] strategies refer to methods where building blocks with four connecting sites linked with linkers possessing two or four connecting sites, respectively. Most COFs obtained by these approaches possess two-dimensional topological structures, with only a few reported examples of three-dimensional configurations.[22–25] The topological structures reported for Pc-COFs are schematically depicted in Fig. 2. For instance, Ding *et al.* adopted a [4 + 2] strategy by employing electron-withdrawing nickel phthalocyanine derivatives (Pc-6) as building blocks and electron-deficient benzothiadiazole (L-36) as linking groups to synthesize a 2D COFs with n-type channels. The combination between the C_4-symmetric phthalocyanine block and C_2-symmetric linker results in tetragonal COFs with a **sql** topological structure.[26]

In addition, Pc-COFs could be constructed *via* a [4 + 4] method, which also yields an **sql** network. For example, Yue *et al.* rationally designed and synthesized novel ultra-stable bimetallic polyphthalocyanine COFs by a nucleophilic aromatic substitution reaction between octahydroxyphthalocyanine (Pc-9, Pc-37) and hexafluorophthalocyanine (Pc-17). The resulting COFs, specifically $CuPcF_8$-CoPc-COF and $CuPcF_8$-CoNPc-COF, exhibit excellent stability under harsh conditions.[27]

In recent years, 3D COFs with new topologies and more voids have been rapidly enriched. Compared to 2D species, their special pore structures including interconnected channels, high surface areas, low densities, and abundant active sites have been demonstrated to be useful in separation, catalysis, and guest encapsulation.[28] The synthesis of 3D COFs requires high-connectivity polyhedral building blocks or precise control over building block alignment. Although the rigid planar structure of phthalocyanine and its derivatives favors the formation of 2D COFs, it is still feasible to construct 3D Pc-COFs structures by selecting appropriate linker groups. For instance, Han *et al.* chose 1,3,5,7-tetra(4-aminophenyl)adamantine (TAPA) (L-5) with T_d symmetry as the linking group to construct **pts** topological structure by the solvothermal reaction.[29] In another approach, Wang *et al.* utilized the latter strategy to assemble square-planar cobalt(II) phthalocyanine (Pc-9) units into a porous 3D COF, named SPB-COF-DBA, which exhibits a noninterpenetrated **nbo** topology by using tetrahedral spiroborate (SPB) linkages, which were chosen to provide the necessary 90° dihedral angles between neighboring PcCo units.[25] Another noteworthy structure is the Pc-COFs with an shp topology, using a linker bearing twelve connecting sites (L-60) in coordination with phthalocyanine molecules.[24]

Besides choosing the appropriate linkers, it is necessary to select or design phthalocyanine molecules with appropriate functional groups in order to connect with linker units through covalent bonds. Thus, as shown in Fig. 3, phthalocyanine and phthalocyanine derivatives containing aldehyde groups, amino groups, boric acids, hydroxyl groups, carboxyl groups, fluorine, imines and acid anhydrides were carefully chosen to react with appropriately functionalized knots/linkers (illustrated in Fig. 4) for the construction of COFs through forming –B–O–, –C=N–, –C–N– and –C–O– covalent bonds, providing more possibilities for the design and synthesis of Pc-COFs.

3. Synthetic strategies for Pc-COFs

The synthesis of Pc-COFs is simpler than that of other COFs types. The main strategy is to use phthalocyanines containing amino, carboxyl, aldehyde, hydroxyl, anhydride and halogen atoms as the blocks, and react them with appropriately functionalized linkers through various condensation or coupling reactions to obtain Pc-COFs with different structures and properties (Fig. 5). In addition to building blocks and linkers, the crystallinity and porosity of the resulting COFs are also highly dependent on the reaction temperature, reaction time, solvent types, and the concentration of organic compounds.[30–35] Thus, selecting the appropriate reaction medium and reaction conditions is particularly crucial for forming thermodynamic stable crystalline COFs.[36] Currently, solvothermal polymerization reactions has became the most common method to prepare crystalline COFs under mixed solvent conditions.[37,38] Following, the most commonly synthesis path of Pc-COFs materials will be described in detail.

3.1 Imine-linked Pc-COFs

The Schiff base reaction is extensively employed in the constructing Pc-COFs. This process involves the condensation of amino or hydrazide groups with aldehyde groups on monomers (Fig. 5a), forming imine linkages that confer high intrinsic conductivity and accessible active sites to the resulting COFs. These characteristics bridge the gap between homogeneous and heterogeneous electrocatalysis.[39–41] In 2024, Teng *et al.* proposed a bipyridine covalent immobilization strategy with the assistance of Pc-COFs platform linked by imine. When the bipyridine groups (BPy) are introduced into the COFs backbone, the metals such as Cu can be coordinated into the layered pore structure, which suppress the leaching agglomeration effect

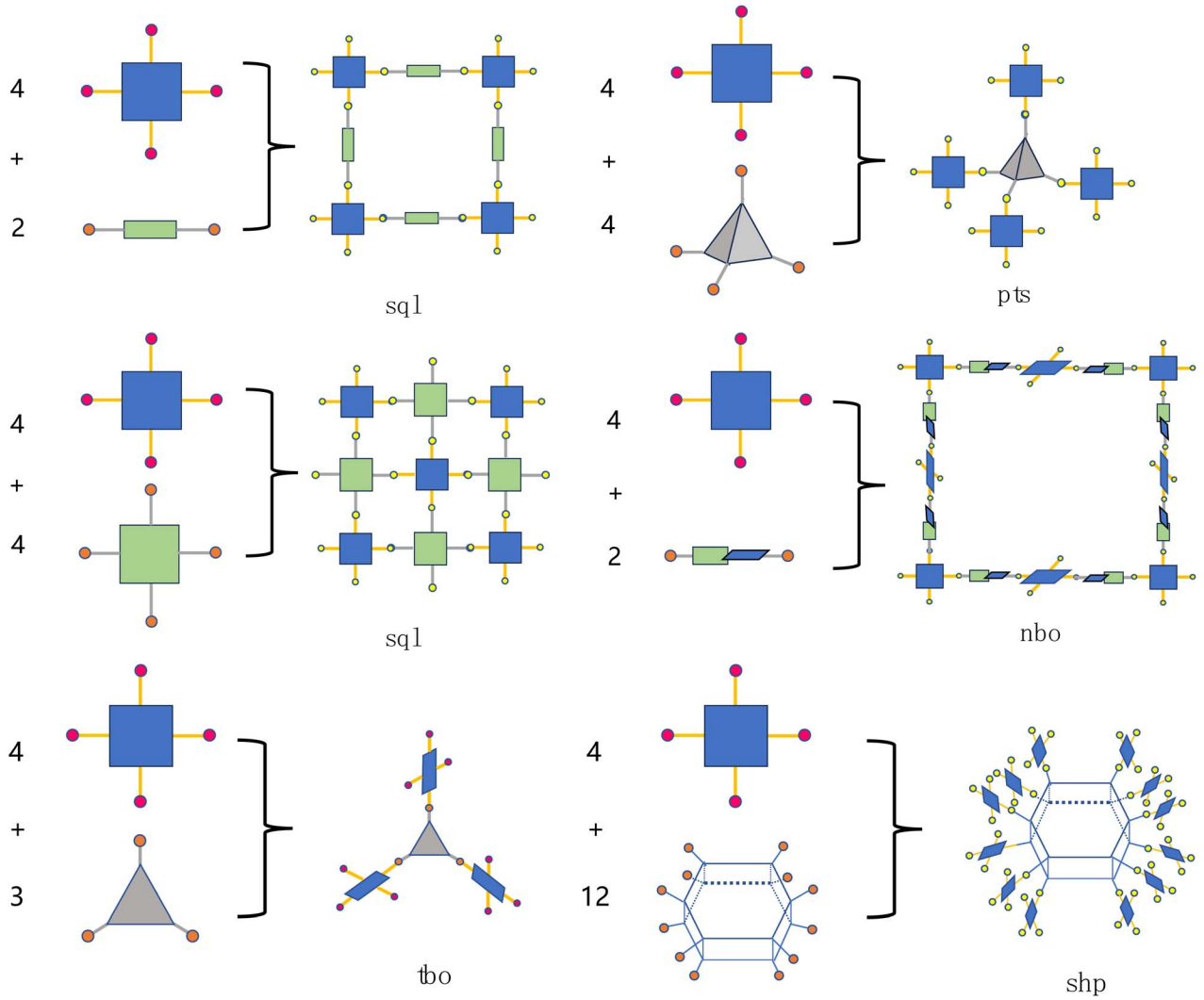

Fig. 2 Synthetic strategies for assembling topologically specific Pc-COFs (quadrilaterals, triangles, and polyhedra represent the main frameworks of the building blocks and linkers, while circles denote the functional groups involved in the reaction, as well as the resulting linkages).

whilst improve the conductivity of bare COFs (Fig. 6).[39] In 2023, Tian *et al.* produced a series of bimetallic Pc-COFs, denoted as NiPc-DFP-MCOF (M = Ni and Co), by assembling 2,3,9,10,16,17,23,24-octaamino-phthalocyaninato nickel(II) (NiPc-8NH_2) with 2,6-diformylphenol (DFP). The synergistic combination of NiPc and metal-ions-coordinated salphen pockets (M-N_2O_2) can endow these materials with enhanced CO_2 adsorption/activation capacity, a built-in electric field effect, and remarkable photosensitivity, leading to superior performance in light-assisted electrocatalytic CO_2RR.[42]

3.2 Imide-linked COFs

Leveraging the planar structure of phthalocyanine molecules, constructing imide-linked covalent organic frameworks has emerged as a highly effective strategy (Fig. 5b). The imide linkages formed by the condensation of anhydride and amino groups not only extend the conjugated system of the phthalocyanines but also significantly enhance the electrocatalytic activity of the resulting COFs.[43] For instance, in 2022, Yuan *et al.* fabricated two novel coupled phthalocyanine-porphyrin COFs, namely Type 1:2 (CoPc-2H_2Por) or Type 1:1 (CoPc-H_2Por), *via* imidization reaction. Due to their adjustable architecture and porous feature, these materials have been applied as potential electrocatalysts for CO_2RR.[44] Further advancing this approach, Zhang *et al.* designed two bifunctional imide-linked covalent organic frameworks through assembling Pc and Por by non-toxic hydrothermal methods in pure water to realize the above catalytic reactions (Fig. 7). For the first time, this work achieves the rational design of bifunctional COFs for coupled heterogeneous catalysis, opening a new avenue for the development of crystalline porous catalysts.[45]

3.3 Piperazine-linked COFs

Ketone ligands are commonly employed in the synthesis of conductive organic materials and have wide applications in electrochemical progresses. 2D conductive COFs with extensive planar π-conjugation have been developed, demonstrating high intrinsic electrical conductivity suitable for electronic devices

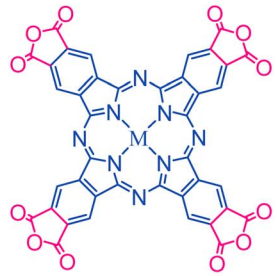

Pc-1(**M**=H), **Pc-2**(**M**=Co)
Pc-3(**M**=Ni), **Pc-4**(**M**=Cu)
Pc-5(**M**=Zn)

Pc-6(M= Ni), **Pc-7**(M= Cu)
Pc-8(M= Zn), **Pc-9**(M= Co)
Pc-10(M= Nb), **Pc-11**(M= H)

Pc-12(M= Cu), **Pc-13**(M= Ni)
Pc-14(M= Co), **Pc-15**(M= **Zn**)

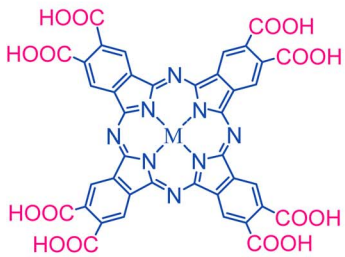

Pc-16(M= Ni)

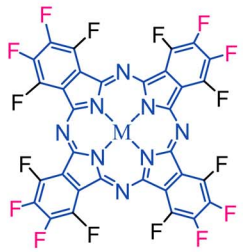

Pc-17(M= Cu), **Pc-18**(M= Co)
Pc-19(M= Fe), **Pc-20**(M= Ni)

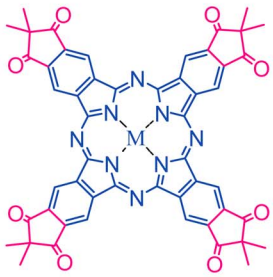

Pc-21(M=H), **Pc-22**(M= Co)

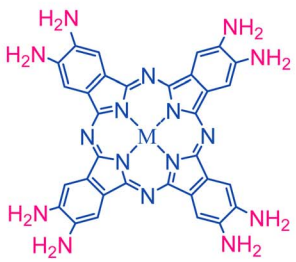

Pc-23(**M**= Ni), **Pc-24**(M= Cu)
Pc-25(M= Zn), **Pc-26**(M= Co)
Pc-27(M= Fe)

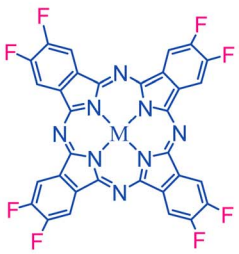

Pc-28(M= Ni)

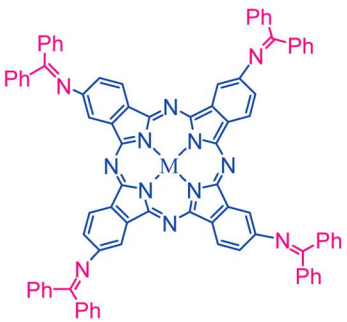

Pc-29(M= Fe), **Pc-30**(M= **Co**)
Pc-31(M= Ni), **Pc-32**(M= **Cu**)
Pc-33(M= Zn), **Pc-34**(M= Mn)

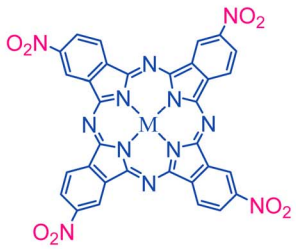

Pc-35(M= Ni)
Pc-36(M= Ce)

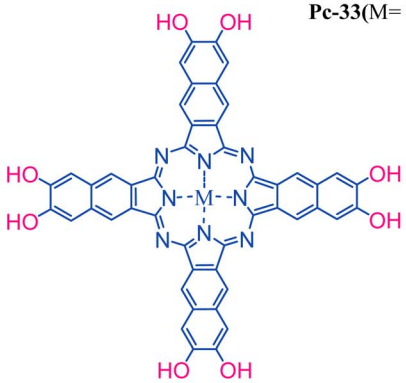

Pc-37(**M**= Co)

Fig. 3 Phthalocyanine building blocks reported.

and chemical sensing.[46,47] Taking these into account, nickel phthalocyanine was integrated into an intrinsically conductive piperazine-linked conjugated 2D COF (NiPc-COF) with high stability for the enhanced CO_2RR in water (Fig. 8). The NiPc-COF nanosheets achieved highly selective reduction of CO_2 into CO under aqueous conditions with a positive onset potential at −0.55 V *versus* the reversible hydrogen electrode (RHE).[48] In 2023, Zhong *et al.* synthesized a series of 2D-COFs

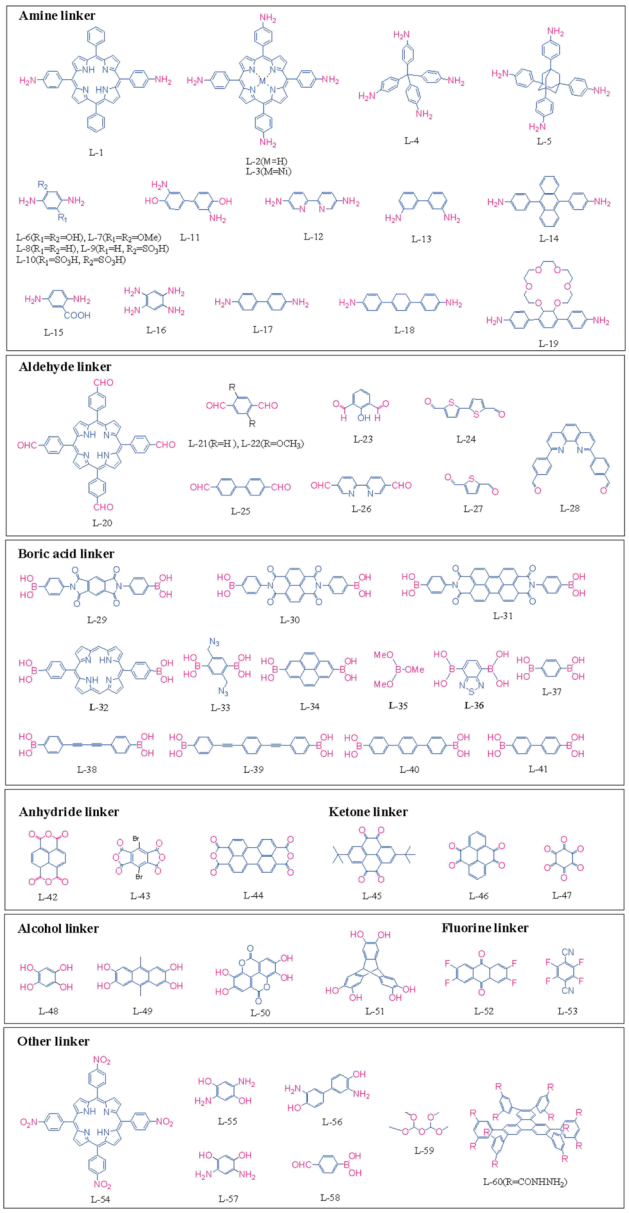

Fig. 4 Linkers containing different binding groups.

based on metal-phthalocyanine (M = Fe, Co, Ni, Mn, Zn, and Cu) and pyrene units bonded by pyrazine linkages (Fig. 5c). These materials simultaneously enhanced both the activity and selectivity for the electrochemical nitrogen reduction reaction (NRR) to ammonia, while also elucidating the influence of different metal centers on the catalytic performance.[49]

3.4 Borate-linked COFs

Boric acid and polyphenol compounds can be used to construct COFs with two-dimensional or three-dimensional structures by polycondensation (Fig. 5d). These COFs have unique chemical structure and properties, such as excellent crystallization, low density, high specific surface area and strong structural designability, and become one of the research hotspots.[50–52] In 2012, Dichtel *et al.* developed a series of 2D zinc phthalocyanine (ZnPc) COFs featuring expanded diagonal pore widths of 2.7, 3.4, 4.0, and 4.4 nm. They achieved this by utilizing the longest molecular linkers ever incorporated into a COF structure (Fig. 9). The team carried out the synthesis in sealed glass ampoules at 120 °C for 72 hours, using dioxane/MeOH mixtures in varying ratios (2 : 1, 3 : 1, 5 : 1), which reproducibly yielded the products as insoluble microcrystalline powders.[53]

The B–O covalent bond in borate-connected COFs gives the material high temperature resistance, but such COFs are also vulnerable to moderate nucleophiles such as water, resulting in the hydrolysis of B–O covalent bonds, which leads to the collapse of pores. Therefore, special attention needs to be paid to protecting boracic-linked COFs from moisture during synthesis and application. The direct formation of boronate esters from protected catechols presents an attractive alternative for COFs synthesis, because the protecting groups can decrease the compound's polarity, prevent autoxidation and confer enhanced solubility. In 2012, Spitler *et al.* reported a new general method for the synthesis of boronate ester-linked COFs avoiding the direct use of insoluble and unstable polyfunctional catechol reactants. Pc-PBBA COF was synthesized by combining Pc, 1,4-phenylenebis (PBBA) and $BF_3 \cdot OEt_2$ in a 1 : 1 mixture of mesitylene and 1,2-dichloroethane (DCE) in a flame-sealed glass reaction vessel, heating at 120 °C for six days. The crude product was isolated by filtration and purified with yield 48%.[54]

3.5 Dioxin-linked COFs

Introducing dual-metal atom centers into COFs has emerged as an effective approach for enhancing sensing and catalytic capabilities by optimizing their electronic structures.[55] This approach utilizes two distinct metal-linked central building blocks to create dual-metal ion active sites in Pc-COFs.[56] Considering that phthalocyanine molecules can act as building units as well as linkers, researchers have successfully condensed phthalocyanine derivatives bearing two different substituents to obtain COFs materials with dual metal centers. In 2021, Huang *et al.* rationally designed and synthesized new kinds of ultrastable bimetallic polyphthalocyanine COFs. Benefiting from an eclipsed stacking mode that enables high-speed electron transfer, the bimetallic CuPcF8-CoPc-COF and CuPcF8-CoNPc-COF exhibited excellent robustness under harsh conditions (Fig. 10), leading to outstanding activity, selectivity, and stability in the electrocatalytic reduction of CO_2 in an aqueous system.[27] In the same year, using the same synthesis strategy as above, Chen *et al.* designed and synthesized another dioxin connected 2D COF material with CuPc $[OH]_8$ and $NiPcF_8$ as building units. The bimetallic COF-CuNiPc with an asymmetric synergistic effect achieves a fast adsorption/desorption process to NO_2.[57]

3.6 Other linkages

Apart from the main linkage group mentioned above, several other types of linkage groups (Fig. 5e) can also be used to construct Pc-COFs, including imidazole, oxazine, and azo groups.[58–60] In 2024, Zhang *et al.* successfully prepared a family of high crystalline benzimidazole-linked Cu(II)-phthalocyanine-based COFs powders and films by a transfer dehydrogenation

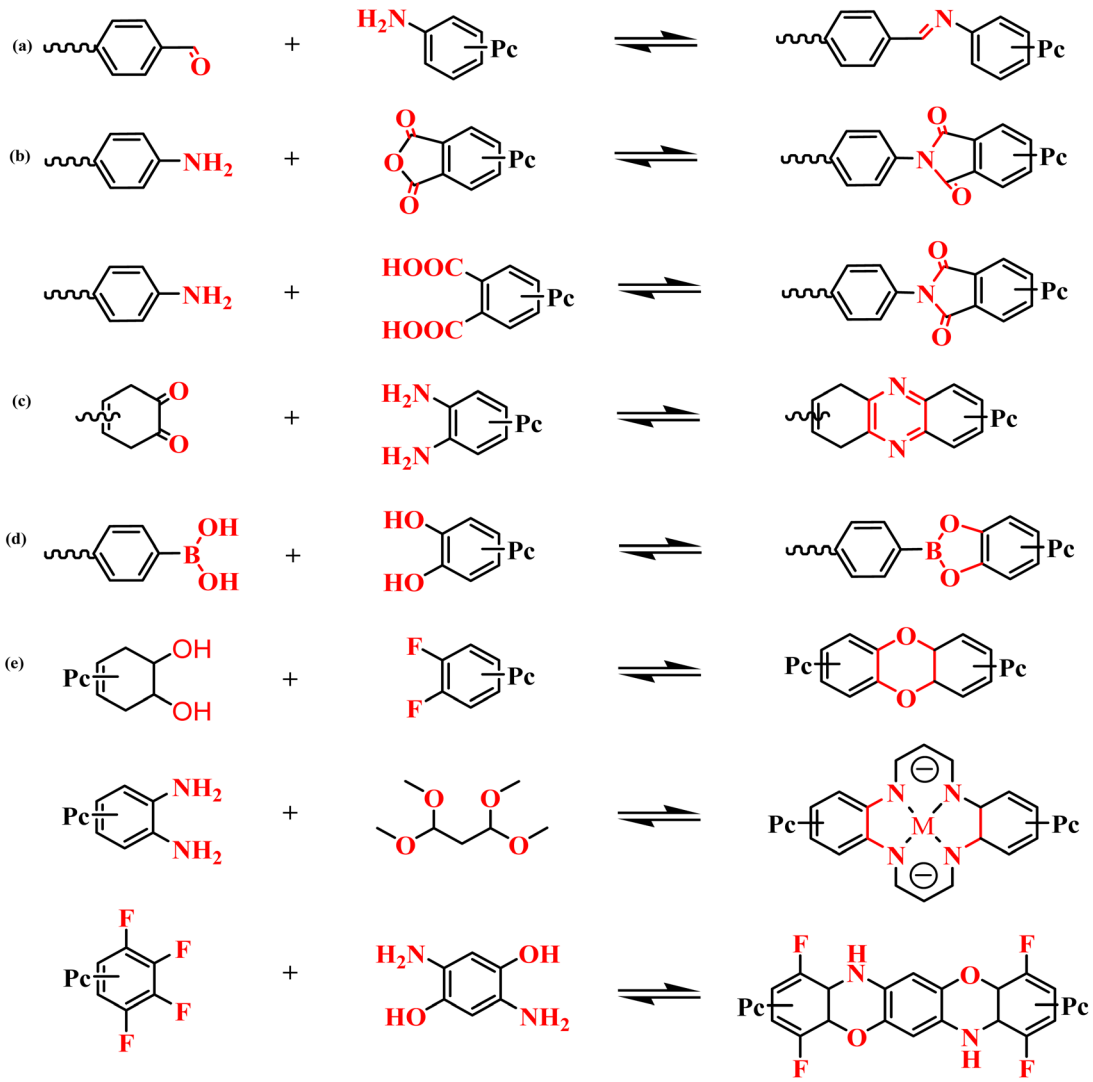

Fig. 5 Different connection methods in the synthesis strategy: (a) imine-linked, (b) imide-linked, (c) phenazine-linked, (d) borate-linked and (e) other linkages.

method with *N*-benzylideneaniline (BA) as a mild reagent (Fig. 11). Both of these new BICuPc-COFs films showed high electrical conductivity (0.022–0.218 S m^{-1}), higher than most of the reported COFs materials.[61] In 2024, three kinds of Pc-COFs, NA-NiPc (4-nitronickel phthalocyanine + 4-aminonickel phthalocyanine), PPDA-NiPc (4-nitronickel phthalocyanine + *p*-phenylenediamine) and DAB-NiPc (4-nitronickel phthalocyanine + 4,4′-diaminobiphenyl), with different pore sizes were synthesized by a catalyst-free coupling reaction (Fig. 12). Moreover, the use of the NA-NiPc, PPDA-NiPc and DAB-NiPc electrodes in sodium-ion batteries also display excellent behaviors, such as high capacities, stable cycling performances and excellent rate capabilities.[62]

The presence of multiple active sites in electrosynthesis reactions has been shown to significantly enhance reaction selectivity and efficiency.[63–65] As a result, Cu-phthalocyanine (CuPc) has attracted considerable attention due to its unique electrocatalytic properties.[66–69] Studies indicate that CuPc can undergo partial *in situ* transformation into composite metal catalysts with nanocluster loadings, providing new avenues for optimizing catalytic performance.[70] To further enhance catalytic performance, Yang *et al.* designed and synthesized a series of CuPc-COFs with dioxin, piperazine and oxazine linkage, separately (Fig. 13). The distinctive structure of CuPc-COFs anchors the partially formed Cu clusters and facilitates synergy with the phthalocyanine Cu sites. This Cu-organic interface synergy significantly enhances the selectivity for C_{2+} products and acetate by optimizing the electronic structure, promoting charge separation, and improving the adsorption and conversion of reaction intermediates.[70–72]

Besides the two-step synthesis method, which involves first synthesizing phthalocyanine monomers and then selecting suitable linkers to construct COFs, another important strategy is to obtain Pc-COFs directly from small molecules.[73] In the process, small molecules act as both the building units of phthalocyanine monomers and the linkers, this method can effectively improve

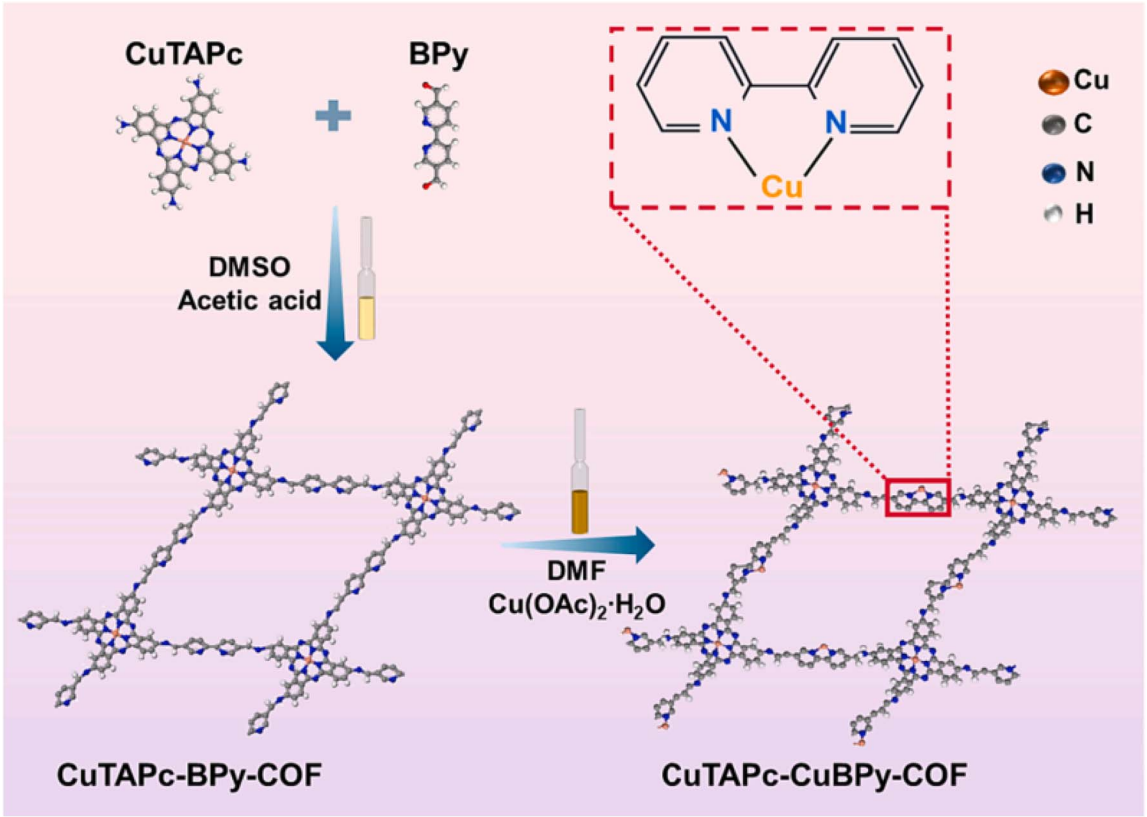

Fig. 6 Schematic illustration of CuTAPc-BPy-COF and CuTAPc-CuBPy-COF materials. Reprinted with permission from ref. 39. Copyright 2023 Elsevier Inc.

the synthesis efficiency. In 2018, Wu *et al.* reported a facile synthetic approach to engineer a cobalt (Co) phthalocyanine-linked polymeric framework with abundant defective sites to facilitate the sluggish CO_2RR in water. To illustrate this strategy briefly, phthalic anhydride, pyromelliticdianhydride, $CoCl_2$, NH_4Cl, urea and $(NH_4)_2Mo_2O_7$, were ground together and then transferred to a muffle furnace. The mixture was kept heating at 220 °C for 3 h to accomplish the polycondensation reaction. The authors proposed that the use of phthalic anhydride as a comonomer could give a rise to the formation of defective sites within the architecture.[74] In 2022, Liu *et al.* selected nitrogen-rich 1,2,4,5-tetracarbonitrile benzene (TCNB) as the sole organic building block, and Cu(II) as anchored at the coordination center, resulting in a stable conjugated two-dimensional network with single-atomic centers under assistance of microwave irradiation.[75] On the basis of small molecular of anhydrides and cyanide compounds, researchers tried to change the molecular length of small molecules to tailor the pore size and surface area of COF. In 2022, Yang *et al.* chosen benzo [1,2-*b*:4,5-*b*′]bis [1,4]benzodioxin-2,3,9,10-tetracarbonitrile (BBTC) and quinoxalino[2′,3′:9,10] phenanthro[4,5-*abc*]phenazine-6,7,15,16-tetracarbonitrile (QPPTC) as the comonomer to fabricate two fully conjugated Pc-based COFs (denoted as BB-FAC-Pc-COF and QPP-FAC-Pc-COF). CO_2 adsorption–desorption measurement discloses their permanent porosity with a Brunauer–Emmett–Teller (BET) surface area of 290 $m^2\ g^{-1}$ for BB-FAC-Pc-COF and 350 $m^2\ g^{-1}$ for QPP-FAC-Pc-COF.[76] Utilizing a mixed-metal salt ionothermal approach, Song *et al.* reported the synthesis of a series of Pc-COFs starting from 1,2,4,5-tetracyanobenzene and 2,3,6,7-tetracyanoanthracene to form the corresponding COFs named M-pPPCs and M-anPPCs, respectively (Fig. 14). The obtained COFs followed the Irving–Williams series in their metal contents, surface areas, and pore volume and featured excellent CO_2 uptake capacities up to 7.6 mmol g^{-1} at 273 K, 1.1 bar.[77]

4. Electrocatalytic and photocatalytic carbon dioxide reduction

Pc-COFs exhibit significant application potential across multiple fields owing to their outstanding characteristics, including high structural designability, broad functional adaptability, customizable topologies, tunable pore size and porosity, diverse building block relationships, varied covalent linkage modes, and large specific surface area.[78] These distinctive properties have enabled COFs to find applications in various areas, such as gas capture,[79] separation,[80,81] energy storage,[82] sensor detection,[83] battery technology,[84] electrocatalysis[85–87] and photocatalysis.[88–90] Among these, electrocatalytic and photocatalytic carbon dioxide reduction represent the most extensively studied applications and have attracted growing research interest, leading to rapid advances in recent years. The following section will provide a detailed overview of recent progress in Pc-COF-based electrocatalytic and photocatalytic CO_2 reduction.

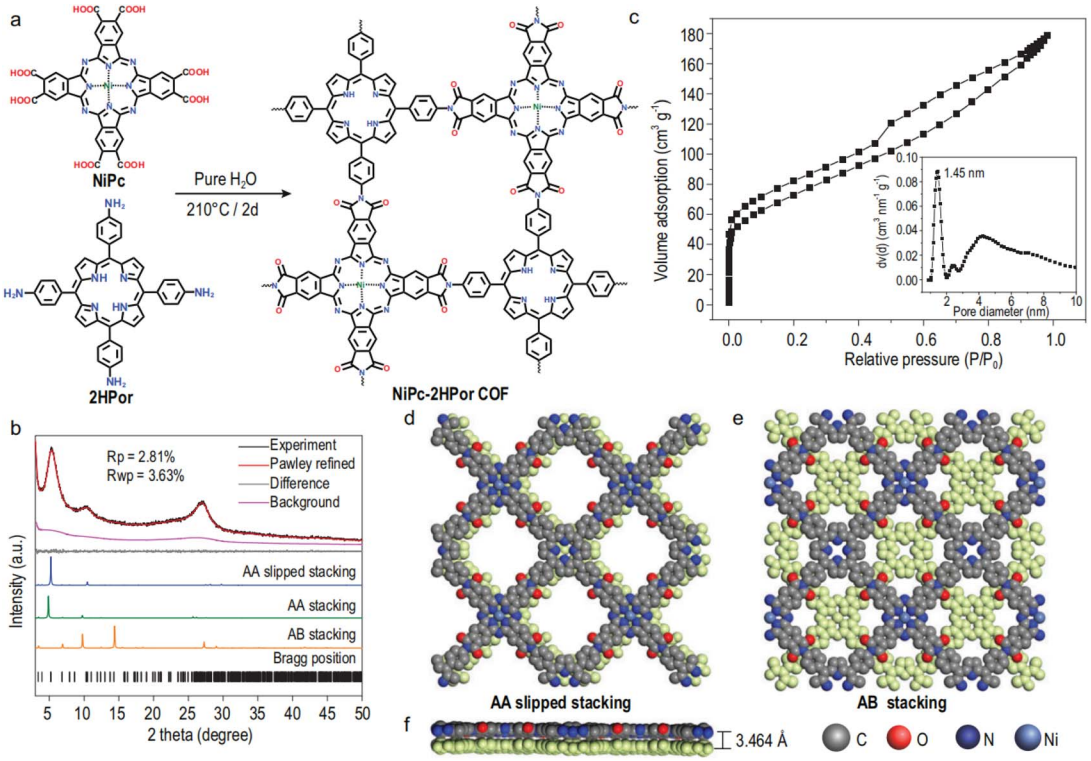

Fig. 7 Schematic illustration for the synthesis of COFs linked by polyimide. (a) Synthesis process of NiPc-2HPor COF. (b) PXRD patterns of NiPc-2HPor COF. (c) Results of N_2 adsorption–desorption results. (d) Simulated crystal structure of AA slipped stacking. (e) Simulated crystal structure of AB stacking. (f) Side perspective of the NiPc-2HPor COF with AA slipped stacking. Republished with permission from ref. 45. Copyright 2023, The Author(s).

4.1 Electrocatalytic carbon dioxide reduction

In recent years, the electrocatalytic carbon dioxide reduction reaction (CO_2RR) has emerged as a promising strategy to address environmental challenges caused by excessive CO_2 emissions.[91–93] The development of suitable electrocatalysts is crucial for the efficient implementation of this process.[94] Covalent organic frameworks, which feature high conductivity, remarkable stability, and uniformly dispersed active sites, show great potential as electrocatalysts to facilitate this conversion.[95] To further improve catalytic performance, researchers have been actively exploring various structural modifications of Pc-COFs. These include varying the linker length, adjusting linker substituents, changing the type and number of central

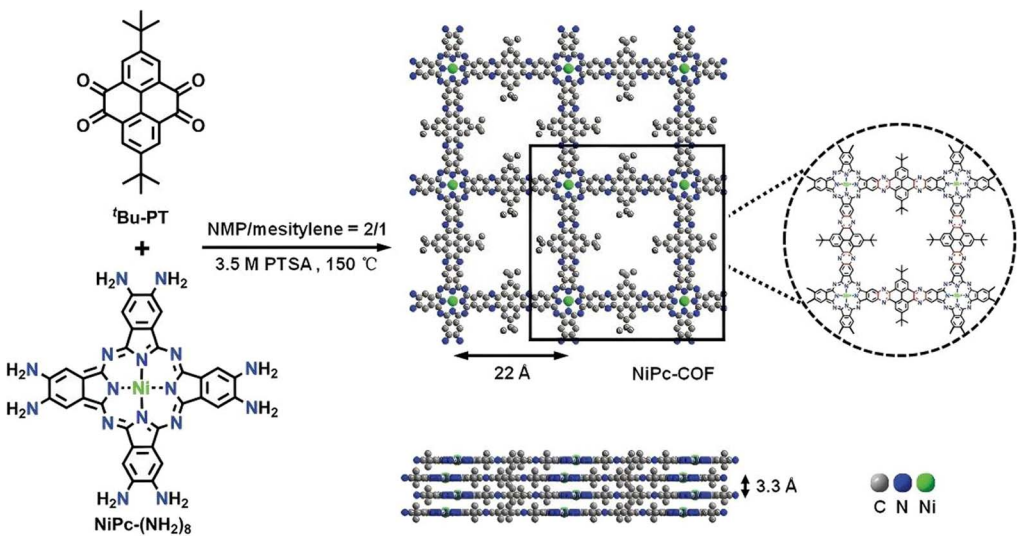

Fig. 8 Synthesis and stacking structure of 2D conductive NiPc-COF. Reprinted with permission from ref. 48. Copyright 2020 Wiley-VCH GmbH.

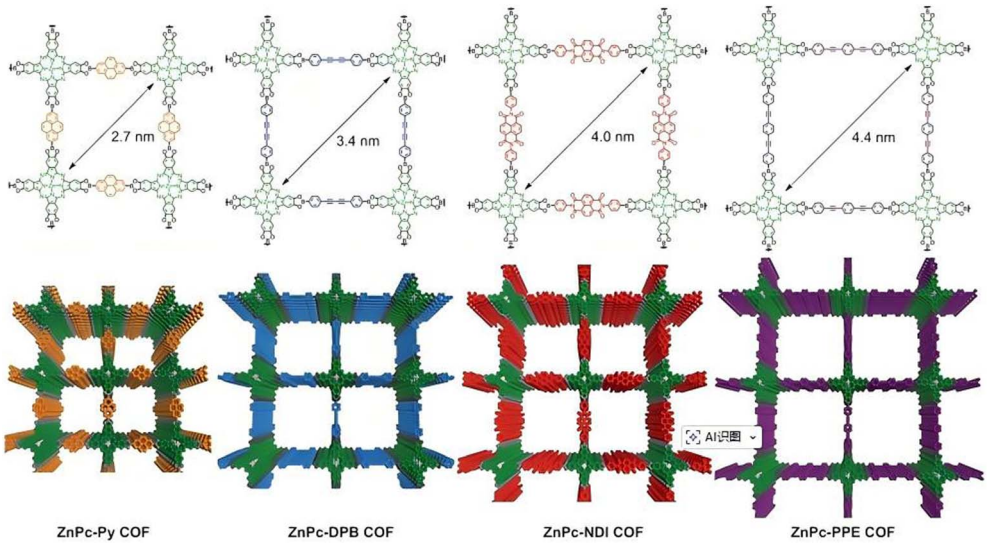

Fig. 9 Chemical and extended structures of the expanded ZnPc COFs. Reprinted with permission from ref. 53. Copyright 2012 Wiley-VCH Verlag GmbH & Co. KGaA, Weinheim.

metal ions, controlling the COF morphology, and developing 3D architectures from 2D frameworks. Table 1 summarizes all reported Pc-COFs materials studied for electrocatalytic CO_2RR.

4.1.1 Altering the length of the linker. For Pc-COFs, the length of the linker is an important factor determining the pore size of the material. By changing the length of the linker, not only can regulate the structure, but also can enhance the catalytic activity of the COFs.[50,98] In 2022, two dimensional Pc-COFs linked by imide, designated as CoPc-PI-COF-1 and CoPc-PI-COF-2, were constructed *via* a solvothermal route. The resultant CoPc-PI-COFs show permanent porosity, thermal stability above 300 °C, and excellent resistance to a 12 M HCl aqueous solution for 20 days. When benchmarked against the CoPc-PI-COF-2 & carbon black electrode, the CoPc-PI-COF-1-based cathode demonstrated superior performance, achieving a larger CO partial current density (j_{CO}) of -21.2 mA cm^{-2} at -0.90 V. This enhancement is attributed to its higher electrical conductivity. Furthermore, this electrode exhibited remarkable

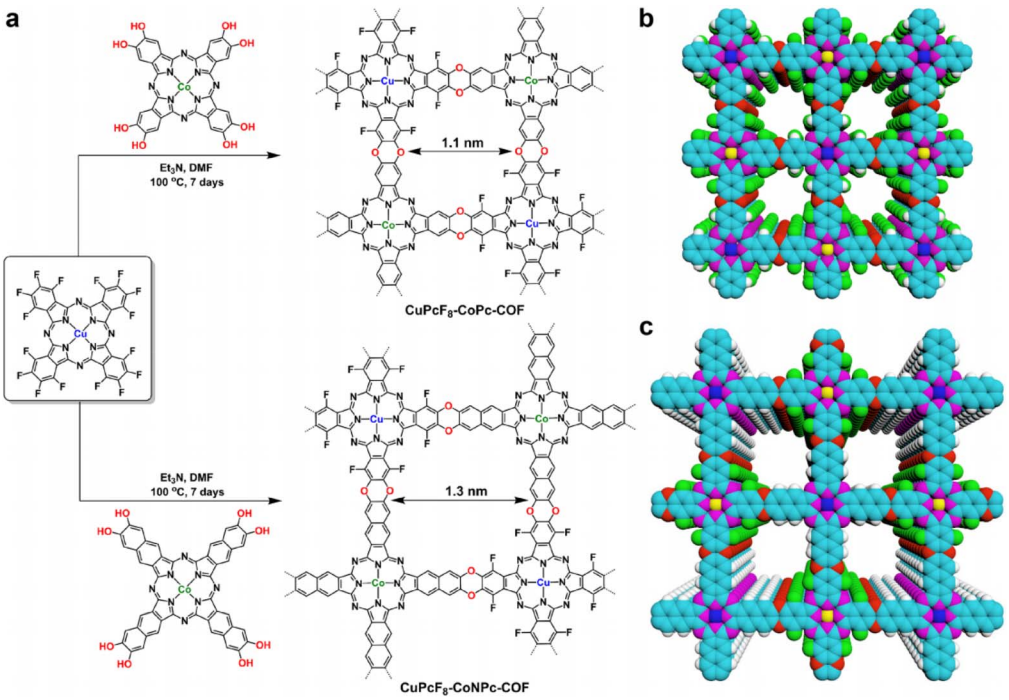

Fig. 10 (a) Design and synthesis of dioxin-linked COFs. (b) Eclipsed stacking of $CuPcF_8$-CoPc-COF and (c) $CuPcF_8$-CoNPc-COF. Reprinted with permission from ref. 27. Copyright 2021 American Chemical Society.

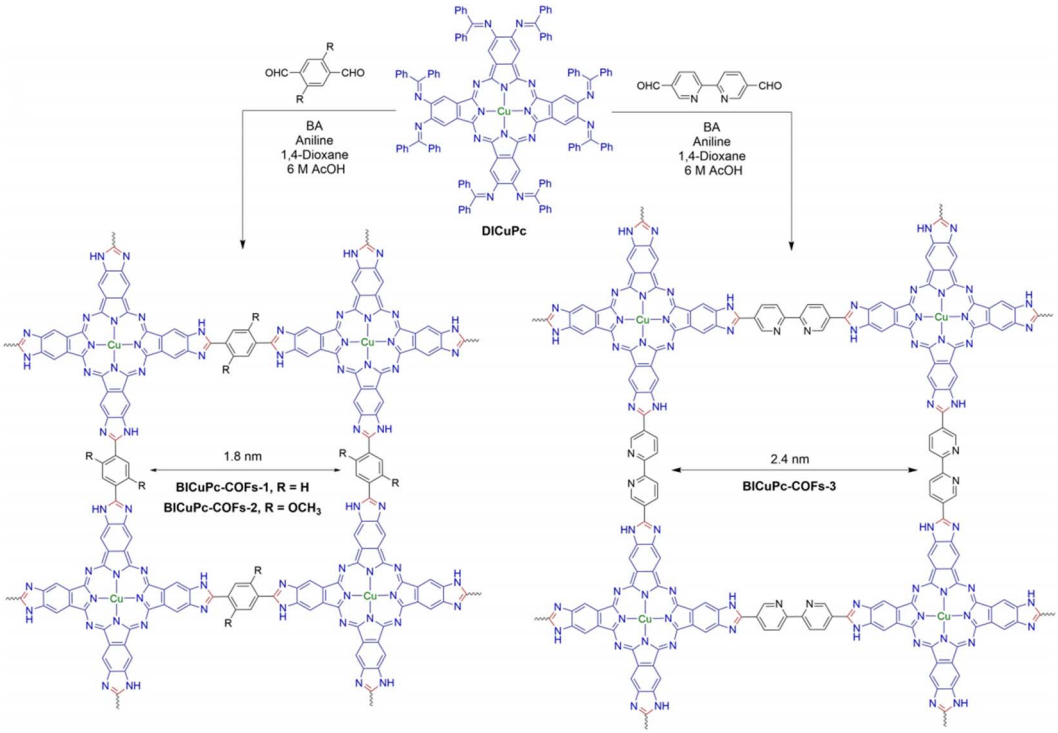

Fig. 11 Synthesis of BICuPc-COFs-1, BICuPc-COFs-2, and BICuPc-COFs-3. Reprinted with permission from ref. 61. Copyright 2024 Wiley-VCH GmbH.

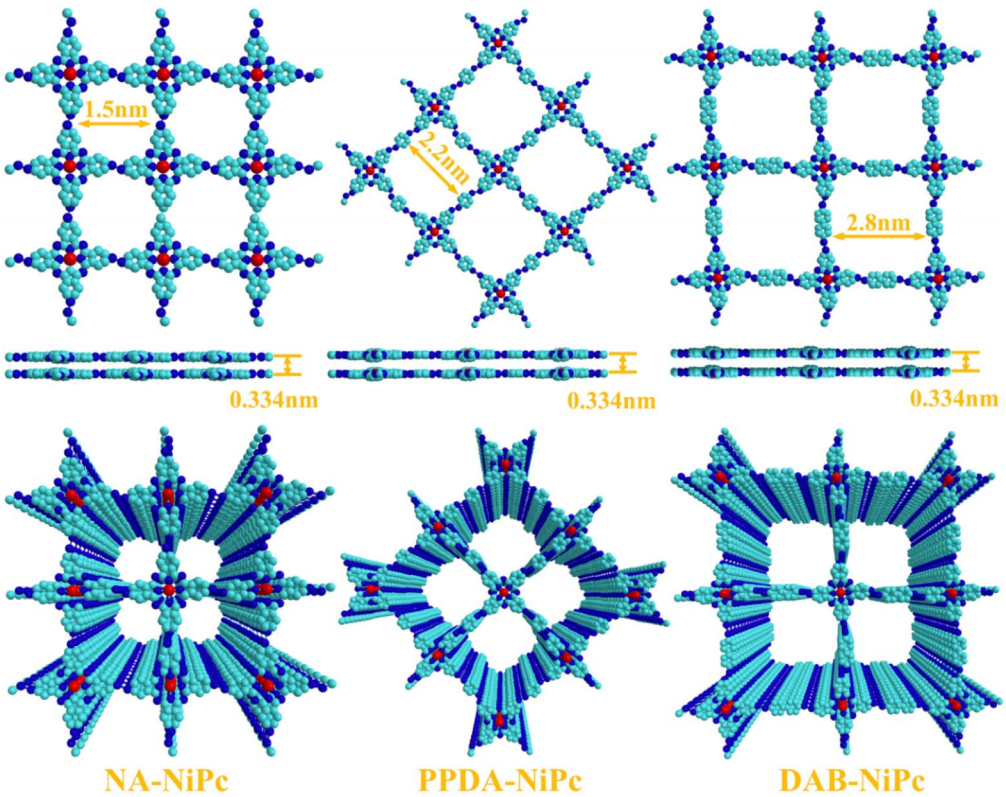

Fig. 12 Geometry optimization of NA-NiPc, PPDA-NiPc and DAB-NiPc with HyperChem release 7.5. Reprinted with permission from ref. 62. Copyright 2021 Elsevier B.V.

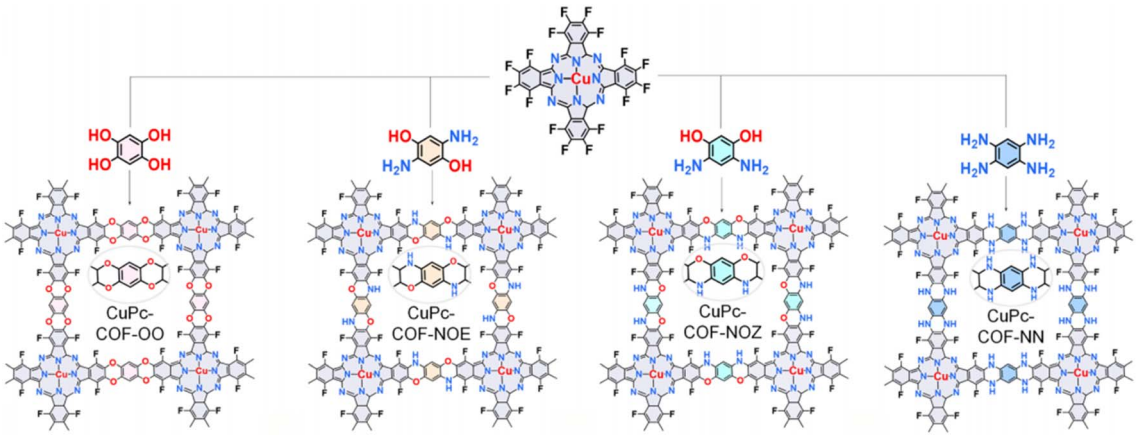

Fig. 13 Schematic diagram of the synthesis of CuPc-COF-OO, CuPc-COF-NOE, CuPc-COF-NOZ, CuPc-COF-NN. Reprinted with permission from ref. 72. Copyright 2025 American Chemical Society.

durability and efficiency over a 40 hour test at −0.70 V, as evidenced by a high turnover number (TON) of 277 000 and a turnover frequency (TOF) of 2.2 s^{-1} (Fig. 15). These findings underscore the significant promise of 2D porous crystalline solids in electrocatalytic applications.[98] In 2018, Yao *et al.* used cobalt phthalocyanine as the building unit and selected PBBA (1,4-phenylene diboronic acid), bPBBA (1,4-biphenylene diboronic acid), and tPBBA (1,4-biphenyltriboronic acid) as the linking groups to construct three types of Pc-COFs (Fig. 16). The results indicate that this series of covalent organic frameworks has emerged as promising candidate catalysts for carbon dioxide reduction, owing to their synergistic effect in storage and catalytic functions. More importantly, by incorporating a storage function, this COF design can increase the concentration of carbon dioxide around the catalytic center to 97.7 times in a conventional aqueous solution environment. This concentration increase effectively reduces the reduction activation energy (the overpotential decreases from 0.39 V to 0.27 V), and significantly improves the yield. Both of these indicators have achieved significant breakthroughs compared to recent reports.[50]

The experimental results demonstrate that the porosity of COF materials can be tuned by varying the linker length, which enhances the local concentration of CO_2 at the active sites and improves catalytic activity. However, longer linkers concurrently reduce the electrical conductivity of these sites, ultimately impairing catalytic performance. Consequently, the design of COF structures must strike a balance between linker length and electrical conductivity.

4.1.2 Adjusting the substituents of the linker. Established strategies for enhancing the performance of CO_2RR include improving CO_2 adsorption/activation, stabilizing reactive intermediates, and reducing the surface work function of the catalyst.[103,104] Notably, for the strategy of enhancing CO_2 adsorption/activation, beyond pore size regulation, the introduction of electron-rich building units into covalent organic frameworks serves as an effective approach. Hence, modifying the substituents on the linkers also presents a viable method for

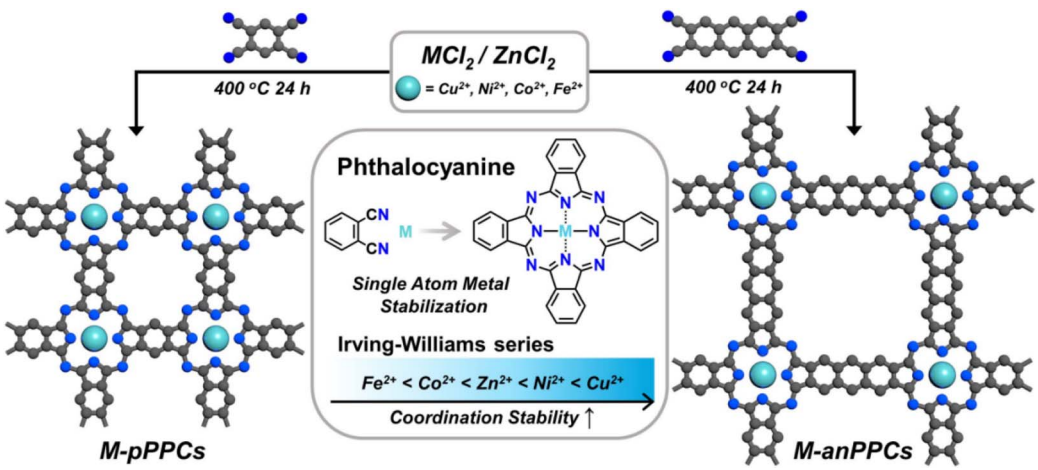

Fig. 14 Schematic representation of the mixed-metal salt approach towards the synthesis of metallophthalocyanine covalent organic frameworks. Reprinted with permission from ref. 77. Copyright 2023 The Authors.

Table 1 Phthalocyanine-based COFs applied for electrocatalytic carbon dioxide reduction reactions[a]

COFs	Monomers	Topology	Linker group	Synthesis condition	Faradaic efficiency (%)	Current density (mA cm^{-2})	Potential (V *vs.* RHE)	Ref.
CuPcF8-CoPc-COF	Pc-17 and Pc-9	sql	Dioxin	Et_3N/DMF, 100 °C, 168 h	91	16.50	−0.70	27
CuPcF8-CoNPc-COF	Pc-17 and Pc-37	sql	Dioxin	Et_3N/DMF, 100 °C, 168 h	97	15.20	−0.62	
NiPc-DFP-Co	Pc-23 and L-23	sql	Imine	MeOH, 24 h	99.86	−12.43	−0.90	42
NiPc-DFP-Ni	Pc-23 and L-23	sql	Imine	MeOH, 24 h	97.81	−9.10	−1.10	
CoPc-2H_2Por	Pc-2 and L-1	sql	Imide	NMP/1-butanol/isoquinoline, 180 °C, 168 h	95	−8.1	−5.5	44
CoPc-H_2Por	Pc-2 and L-2	sql	Imide	NMP/1-butanol/isoquinoline, 180 °C, 168 h	94	−6.1	−5.5	
NiPc-NiPor COF	Pc-16 and L-3	sql	Imide	Pure H_2O, 210 °C, 48 h	98.12	6.14	2.1	45
NiPc-COF	Pc-23 and L-45	sql	Piperazine	NMP/mesitylene/PTSA, 150 °C, 120 h	94.40	54	−0.5	48
Co-Pc-PBBA	Pc-22 and L-37	sql	Borate	—	—	—	0.13	50
Co-Pc-bPBBA	Pc-22 and L-41	sql	Borate	—	—	—	—	
Co-Pc-tPBBA	Pc-22 and L-40	sql	Borate	—	—	—	—	
NiPc-Im-COF	Pc-23 and L-25	sql	Imidazole	NMP/mesitylene, 170 °C, 144 h	90	267	−0.8	85
NiPc-OH-COF	Pc-3 and L-6	sql	Imide	NMP/mesitylene/isoquinoline, 180 °C, 120 h	∼100	−39.2	−1.1	96
NiPc-OMe-COF	Pc-3 and L-7	sql	Imide	NMP/mesitylene/isoquinoline, 180 °C, 120 h	99.3	−20.3	−1.1	
NiPc-H-COF	Pc-3 and L-8	sql	Imide	NMP/mesitylene/isoquinoline, 180 °C, 120 h	95	−18	−1.1	
HPc-PI-COF-3	Pc-1 and L-5	pts	Imide	NMP/*n*-BuOH/isoquinoline, 180 °C, 120 h	—	—	—	97
CoPc-PI-COF-3	Pc-2 and L-5	pts	Imide	NMP/*n*-BuOH/isoquinoline, 180 °C, 120 h	96	−31.7	−0.9	
CoPc-PI-COF-1	Pc-2 and L-8	sql	Imide	NMP/*n*-BuOH/isoquinoline, 180 °C, 120 h	97	—	−0.8	98
CoPc-PI-COF-2	Pc-2 and L-17	sql	Imide	NMP/*n*-BuOH/isoquinoline, 180 °C, 120 h	96	—	−0.8	
2D-NiPc-COF	Pc-3 and L-12	sql	Imide	NMP/isoquinoline, 180 °C, 120 h	90	−13.97	−0.9	99
3D-NiPc-COF	Pc-3 and L-4	pts	Imide	NMP/isoquinoline, 180 °C, 120 h	97	−8.25	−0.8	
NiPC-NH-TFPN-COF-NH_2	Pc-23 and L-53	sql	Piperazine	Dioxane/Et_3N, 120 °C, 72 h	99.6	—	−1.0	100
NiPC-NH-TFPN-COF-COOH	Pc-23 and L-53	sql	Piperazine	Dioxane/Et_3N, 120 °C, 72 h	71.4	—	−1.0	
NiPc-TFPN COF	Pc-6 and L-53	sql	Dioxin	DMA/E_3tN, 150 °C, 72 h	99.8 (±1.24)	−14.1	−0.9	101
CoPc-TFPN COF	Pc-9 and L-53	sql	Dioxin	DMA/E_3tN, 150 °C, 72 h	96.1 (±1.25)	−10.6	−0.9	
ZnPc-TFPN COF	Pc-8 and L-53	sql	Dioxin	DMA/E_3tN, 150 °C, 72 h	22.9	—	−0.9	
CoPc-PDQ-COF	Pc-26 and L-46	sql	Piperazine	DMAc/ethylene glycol/acetic acid, 200 °C	96	49.4	−0.66	102

[a] DFP – 2,6-diformylphenol, TFPN – tetrafluorophthalonitrile, PTSA – *p*-toluenesulfonic acid, NMP – *N*-methyl-2-pyrrolidone, PDQ – 4,5,9,10-pyrenediquinone, PI – polyimide.

boosting catalytic performance. In 2024, Xie *et al.* demonstrate a strategy for tuning the microenvironment of CO_2RR by learning from the natural chlorophyll and heme. As a result, the addition of $-CH_2NH_2$ can greatly enhance the activity and selectivity of CO_2RR. As proven by experimental characterization and theoretical simulation, the electron-donating group ($-CH_2NH_2$) not only reduces the surface work function of COF, but also improves the adsorption energy of the key intermediate *COOH, compared with the COFs with electron-withdrawing groups (–CN, –COOH) near the active sites.[100]

Furthermore, the substituents on the linkers can also interact *via* weak chemical bonds, which enhances both the stability and electrical conductivity of the COFs. In 2022, Li *et al.* synthesized three COFs by adopting the strategy of changing the substituent of the linker. NiPc-OH-COF exhibits superior stability, especially in strong NaOH, and a high conductivity of 1.5×10^{-3} S m^{-1}, outperforming both NiPc-OMe-COF and NiPc-H-COF. This enhancement is attributed to strong interlayer hydrogen bonds formed between the hydroxyl groups on DB units in adjacent layers.[96]

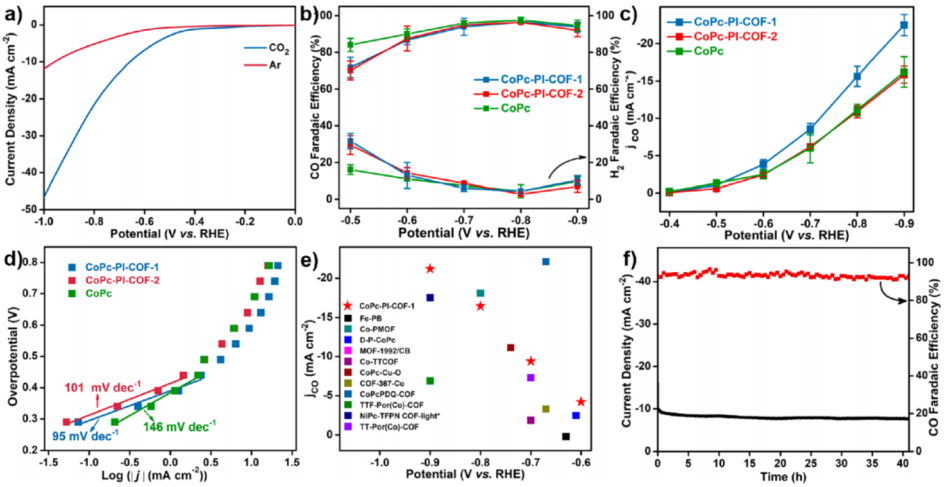

Fig. 15 (a) Faradaic efficiency (b) Partial CO current density (c) Tafel plots (d) of CoPc-PI-COF-1, CoPc-PI-COF-2, and CoPc. (e) Stability test at −0.70 V for 40 h. (f) Comparison of CO partial current densities between CoPc-PI-COF-1 with porphyrin/phthalocyanine electrocatalysts. Reprinted with permission from ref. 98. Copyright 2021 American Chemical Society.

Thus, tailoring the electronic structure of COFs *via* linker substituents (*e.g.*, with electron-donating groups to lower work function and optimize adsorption) and utilizing weak interchain interactions (such as hydrogen bonds) to enhance stability and conductivity together provide a synergistic strategy for enhancing CO_2RR activity and selectivity.

4.1.3 Changing central metal ion. The choice of central metal element directly governs the reduction mechanism. A central Co atom, for example, binds $*CO_2$ and *CO with comparable strength, allowing Co to be readily released as the product. Conversely, systems with central Ni or Cu atoms face a higher energy barrier for *COOH formation, a rate-determining step that imposes a significantly larger onset overpotential (shown in Table 1).[11] To this end, achieving the introduction of bimetallic active sites is a key objective in the development of COF-based electrocatalysts for CO_2RR. In 2022, Yue *et al.* rationally designed and synthesized new kinds of ultrastable bimetallic polyphthalocyanine COFs. The resulting bimetallic $CuPcF_8$-CoPc-COF and $CuPcF_8$-CoNPc-COF displayed considerable activity, selectivity, and stability toward CO_2RR. Computational analysis reveals distinct roles for the metal centers: Co sites show a stronger affinity for the *COOH intermediate, while Cu sites bind *H more favorably. This suggests that Co and Cu serve as the primary active sites for CO_2RR and HER, respectively. Additionally, the Gibbs free energy for *COOH formation and the resulting overpotential are modulated by the specific phthalocyanine units involved. In contrast, Cu atoms exhibit the lowest energy barrier and the highest electron/proton transfer rate during HER. The presence of Cu in $CuPcF_8$-CoPc-COF and CuPcF8-CoNPc-COF is proposed to promote the protonation of $*CO_2$ adsorbed on Co sites, thereby accelerating the overall CO_2RR process.[27]

In 2022, a series of NiPc-DFP-M COFs (M = Ni, Co) were constructed by involving the integration of salphen pockets into the framework (Fig. 17). These materials feature tunable bimetallic centers with distinct coordination spheres, high light sensitivity, and intrinsic electric-field effects, making them highly effective for light-driven CO_2RR. Specifically, the

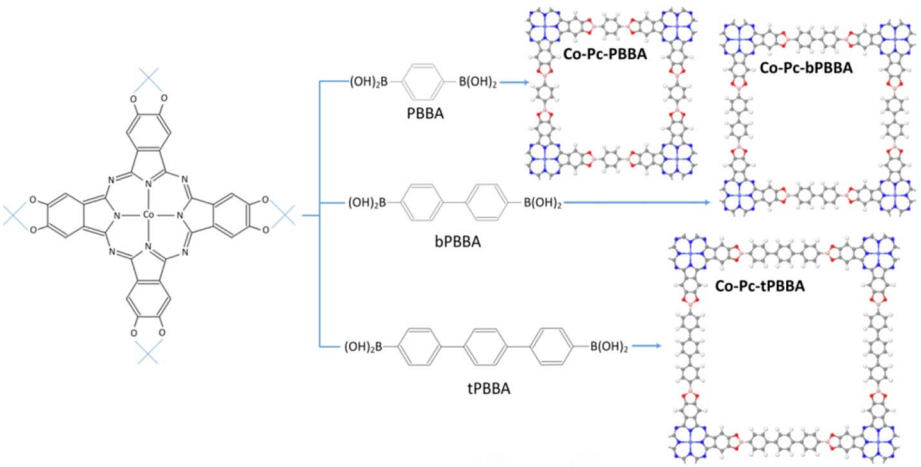

Fig. 16 Atomic structure of the COF series and the corresponding fragment. Reprinted with permission from ref. 50. Copyright 2018 Wiley-VCH.

heterometallic NiPc-DFP-Co COF achieves ~100% faradaic efficiency for CO (FE_{CO}) across a broad potential window −0.7 to −1.1 V and an energy efficiency of ~70% at −0.7 V under illumination, superior to both monometallic and homometallic analogues tested in the dark.[42] The enhanced activity can be attributed to the cooperative interaction of NiPc and Co-salphen units, which notably reduces the energy barrier for the rate-limiting step and promotes electron density, as confirmed by DFT simulations, leading to improved photoelectrocatalytic performance.

4.1.4 Transforming the shape of COFs. Altering the physical form of catalysts is primarily achieved through two approaches. One method involves fabricating them into various nanostructures such as nanoparticles, nanotubes, or nanosheets to increase the number of active sites and enhance catalytic efficiency. The alternative approach entails immobilizing them onto another catalyst support, leveraging synergistic effects between components to improve overall catalytic activity.[17,48] In 2022, two dimensional conductive COF nanosheets composed of Ni-phthalocyanine units linked by pyrazine have been synthesized and applied as an efficient electrocatalyst for CO_2 reduction. The material exhibits superior charge transport and abundant exposed active sites, resulting in CO selectivity exceeding 93% across a broad potential window from −0.6 to −1.1 V, with a peak FE_{CO} of 99.1% at −0.9 V. It delivers a CO partial current density of 35 mA cm^{-2} at −1.1 V, higher than that of conventional insulating COF-based catalysts. Furthermore, the covalent pyrazine linkages endow the framework with remarkable structural integrity, enabling stable performance over 10 hours of continuous operation. This study demonstrates a viable approach to enhance both current density and product selectivity in CO_2RR using 2D conductive COF nanosheets, offering valuable insights for the rational design of advanced porous framework electrocatalysts.[48] Another illustrative example to modify the COFs catalyst is loading it on TiO_2 nanotubes (NTs), and forming a dual-active-site electrochemical catalyst. A Pc-COF, namely CoPc-COF, *in situ* grew on the surface of multilayered NTS, generate the CoPc-COF@TiO_2 NTs composite. Remarkably, the CoPc-COF@TiO_2 NT hybrid demonstrates unprecedented electrocatalytic performance in converting CO_2 and NO_3^- to urea, achieving a record yield of 1205 μg h^{-1} cm^{-2} and a high faradaic efficiency of 49% at −0.6 V (*vs.* RHE), which is attributed to a pronounced synergistic effect between the composite's constituents.[17]

4.1.5 Modifying the structure from 2D to 3D. The density of active sites and the efficiency of substrate diffusion play a critical role in determining the CO_2RR performance of electrocatalysts, as reflected in their turnover number and overall product yield.[103] However, the stacking pattern of two-dimensional COFs, especially the AA stacking mode that is widely adopted for frameworks containing conjugated structures of phthalocyanine units, seems to limit the number of exposed metal ions to a certain extent, thereby reducing the concentration of surface active sites. The use of porous 3D reticular materials serves as a promising strategy to address this issue, as their structure mitigates the aggregation of molecular building blocks, thereby increasing the density of accessible electrocatalytic active sites.[104]

Synthesis of functional 3D COFs with irreversible bond is challenging. In 2022, two 3D imide-bonded COFs were constructed. Structural analyses confirm that both 3D COFs constitute interpenetrated pts-topology networks. Electrocatalytic cathode of CoPc-PI-COF-3 integrated with carbon black demonstrates efficient CO_2-to-CO conversion in $KHCO_3$ aqueous solution, achieving a faradaic efficiency of 88–96% within approximately −0.60 to −1.00 V (*vs.* RHE). The accessible 3D porous framework allows 32.7% of the CoPc subunits to function as active sites, consequently delivering a high CO partial current density (j_{CO}) of −31.7 mA cm^{-2} at −0.90 V (Fig. 18). These values represent a substantial improvement over the high-performing 2D CoPc-PI-COF-1 (5.1% active sites; $j_{CO} = -21.2$ mA cm^{-2}).[97] Meanwhile, Zhang *et al.* discovered by comparing 2D and 3D nickel phthalocyanine-based COFs that 3D-NiPc-COF electrode displays higher CO_2 to CO faradaic efficiency, superior electrocatalytic capacity with the larger partial CO current density and higher turnover number and turnover frequency during the 8 h lasting test.[99] The above example demonstrates that modifying the COF structure from 2D to 3D can effectively increase the surface active sites, leading to enhance the CO_2 reduction catalytic activity.

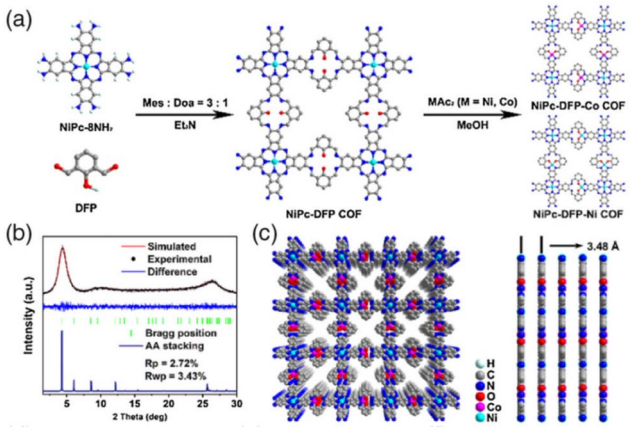

Fig. 17 (a) The syntheses route of NiPc-DFP-M COF (M = Co and Ni). (b) PXRD patterns of NiPc-DFP-Co COF. (c) AA stacking mode for NiPc-DFP-Co COF. Reprinted with permission from ref. 42. Copyright 2023 CCS Chem.

4.2 Photocatalytic carbon dioxide reduction

A key advantage of 2D COFs lies in their extended π-conjugation planar, which promotes broad spectral absorption and shows great potential for driving photocatalytic reactions under infrared light.[22] The phthalocyanine unit, with 18-π-electron planar conjugated array, is a prime example of building block that offers wide-range wavelength absorption and has been extensively utilized in constructing photocatalysts.[19,20] Recent studies have successfully developed various Pc-COFs for applications, such as photocatalytic H_2O_2 generation,[24] CO_2 reduction,[105–108] aerobic oxidation of alkyl benzenes,[90] oxidation of sulfides,[88] photodegradation of dyes,[89] solar steam

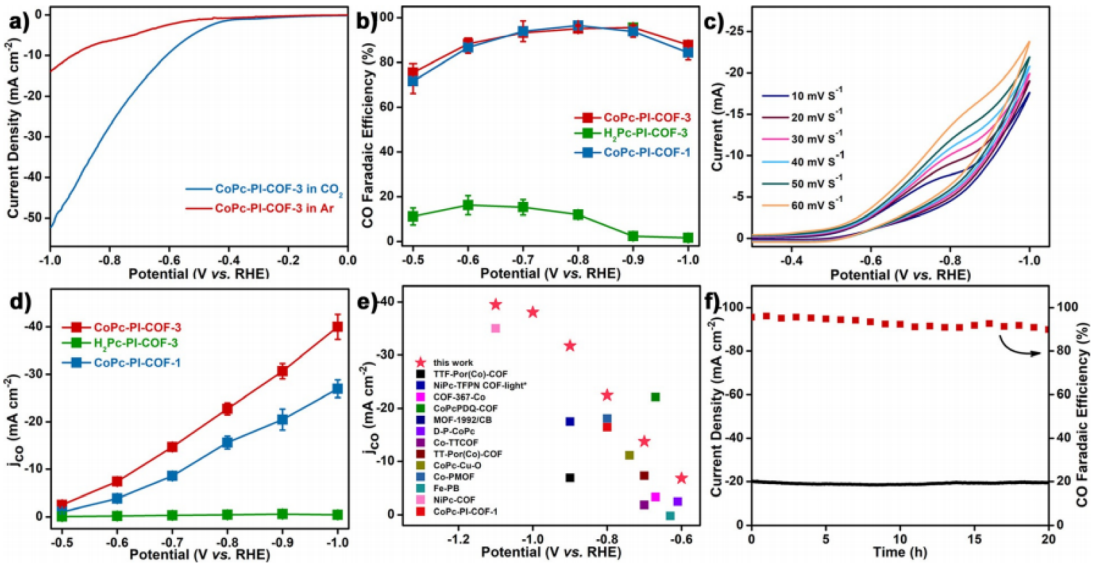

Fig. 18 (a) LSV curves of CoPc-PI-COF-3. (b) Faradaic efficiency diagrams of different COFs electrodes. (c) Scan rate dependence of cyclic voltammetry response of CoPc-PI-COF-3. (d) Partial CO current density of different COFs electrodes. (e) j_{CO} of 3D COF electrocatalyst and of Por/Pc-containing reticular materials performed. (f) Durability performance of 3D COF electrode at −0.80 V. Reprinted with permission from ref. 97. Copyright 2021 Wiley-VCH GmbH.

generators.[109] Table 2 summarizes all reported Pc-COFs materials studied for photocatalytic CO_2RR.

The study found that the local electric field (LEF) has a profound impact on the catalytic process in photocatalysis. Nevertheless, a pivotal challenge lies in the precise construction and manipulation of the electric field microenvironment surrounding active sites. Confronting this challenge, pioneering research has devised multiple approaches to engineer the local structure of active sites, and their divergent photocatalytic performances have been compared in CO_2 reduction reactions, such as designing changing linker,[51,107] designing two metal center,[106,111] or supported on carrier.[89] Zhang *et al.* designed and constructed a cobalt phthalocyanine-containing COF integrated with the host macrocycle 18-crown-6 (Fig. 19). By concentrating K^+ around the Co active site within a 1.6 nm range *via* the interaction between 18-crown-6 ether and K^+, a directionally aligned local electric field (LEF) along the reaction axis was established. Experimental results demonstrated that the addition of K^+ enhanced photocatalytic CO_2 reduction activity by 180%.[111]

In 2024, Luo *et al.* developed an innovative CoPc-Rebpy COF (Fig. 20), which features a Z-scheme molecular heterojunction that enables directional intramolecular charge migration from CoPc to the Re center through Rebpy units for CO_2RR. Under visible light irradiation, the activity of CoPc-Rebpy was significantly enhanced compared to that of CoPc-bpy, which can be attributed to the synergistic effect generated by the Re catalytic site and the electron capture center provided by the CoPc

Table 2 Phthalocyanine-based COFs applied for photocatalytic carbon dioxide reduction reactions[a]

COFs	Monomers	Topology	Linker group	Synthesis condition	CO production	Selectivity (%)	AQE (%)	Ref.
Co-DA-COF	Pc-18 and L-6	sql	Morpholine	Et_3N/dioxane, 120 °C	20.9 mmol g^{-1} h^{-1}	90.5	—	59
Co-DB-COF	Pc-18 and L-11	sql	Morpholine	Et_3N/dioxane, 120 °C	25.7 mmol g^{-1} h^{-1}	92.3	0.65	
EPCo-COF	Pc-18 and L-50	sql	Dioxin	DMF/Et_3N, 120 °C, 72 h	14.1 mmol g^{-1} h^{-1}	85.1	—	106
EPCo-COF-AT	Pc-18 and L-50	sql	Dioxin	DMF/Et_3N, 120 °C, 72 h	17.7 mmol g^{-1} h^{-1}	97.8	—	
NiTAPC-BPMDA COF	Pc-13 and L-43	sql	Imide	DMSO/acetic acid, 120 °C, 24 h	29.65 μmol g^{-1} h^{-1}	98	—	110
CoPc-TPA-CE	Pc-2 and L-19	sql	Imide	NMP/*n*-butanol/isoquinoline, 180 °C, 168 h	7.79 mmol $mmol_{Co}^{-1}$ h^{-1}	95	—	111
CoPc-Rebpy COF	Pc-2 and L-12	sql	Imide	1-Butanol/NMP/isoquinoline, 180 °C, 120h	6680 μmol g^{-1} h^{-1}	83	3.92	112

[a] TPA – *p*-terphenyl diamine, EP – dioxin-linked, BPMDA – 3,6-dibromopyromellitic dianhydride.

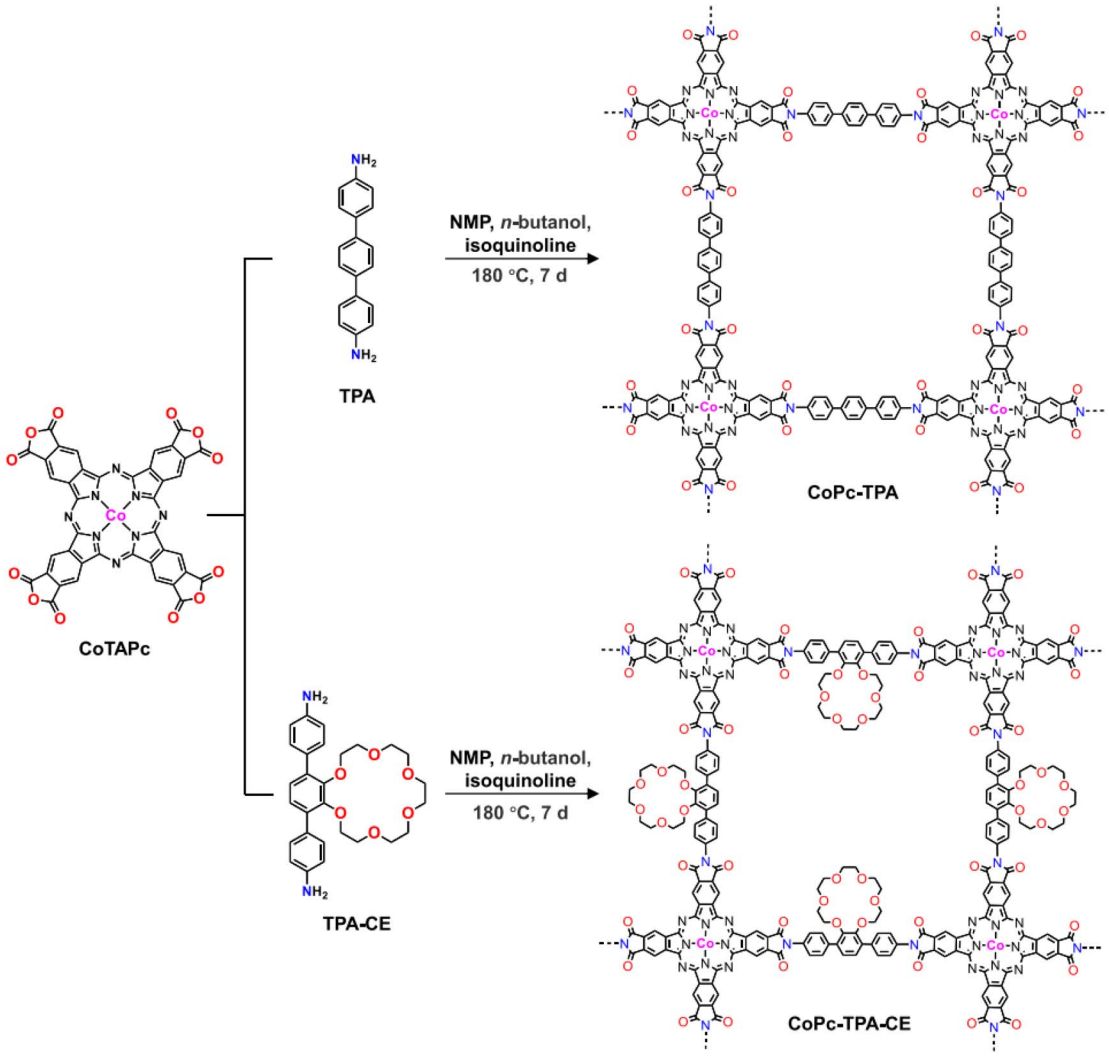

Fig. 19 Schematic representation of the synthesis of CoPc-TPA and CoPc-TPA-CE under solvothermal. Reprinted with permission from ref. 111. Copyright 2025 American Chemical Society.

unit.[112] The above results provide valuable insights into the crucial roles played by the covalent framework and the single-atom bimetal centers (Re and Co) in enhancing the CO_2RR performance. The conjugated framework in COFs enables efficient electron transfer and charge separation, while also enhancing structural stability. Simultaneously, the embedded single-atom metal centers (*e.g.*, Re, Co) provide well-dispersed active sites that concentrate photoexcited charges. Together, these two components work synergistically to boost the catalytic activity, selectivity, and long-term stability of COFs in the CO_2RR process.

The superior CO_2 catalytic activity was attributed to the expanded π-conjugation in the COFs, which enhanced electron delocalization, promoted photogenerated carrier separation, and collectively contributed to an accelerated charge transfer rate. In 2025, Lin *et al.* synthesized two novel morpholine-linked cobalt phthalocyanine-based COFs, Co-DA-COF and Co-DB-COF (Fig. 21). The synergistic effect between the incorporated morpholine bonds and the intrinsic photosensitivity of metal phthalocyanine in the COFs markedly improved photoabsorption and electron transport, thus boosting the overall efficiency of photocatalytic CO_2 reduction. Under comparable conditions, the Co-DB-COF exhibits a CO production rate in the visible spectrum that ranks among the highest reported for COF-based photocatalysts.[59] Lin *et al.* employed Ellagic Acid (EA) along with various perfluorinated metallophthalocyanines ($MPcF_{16}$: M = Co, Ni, Cu) to design and synthesize a series of dioxin-linked metal phthalocyanines (EPM-COF). Remarkably, the photocatalytic CO_2RR performance showed that the engineered EPCo-COF demonstrated a CO productivity of 14.1 mmol g^{-1} h^{-1}.[106]

5. Conclusions and perspectives

Based on the unique structure and properties of Pc-COFs, the research on these compounds has attracted increasing attention. This review provides a detailed introduction to the selection of building blocks and linkers for Pc-COFs, as well as their synthesis strategies. It also focuses on summarizing the application of these materials in electrocatalytic and photocatalytic

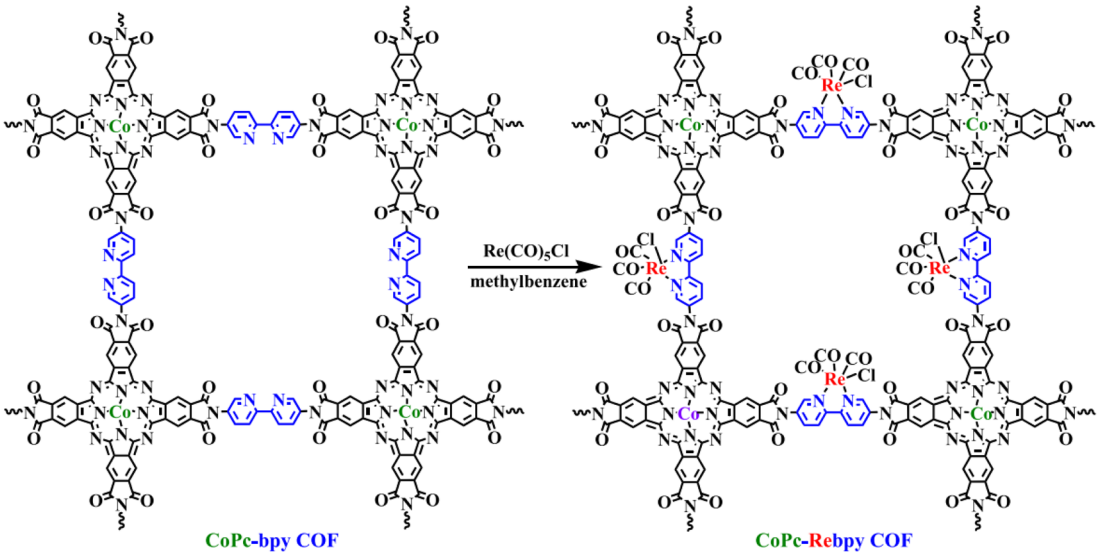

Fig. 20 Synthetic routes and structures of the CoPc-bpy and CoPc-Rebpy COFs. Reprinted with permission from ref. 112. Copyright 2024 American Chemical Society.

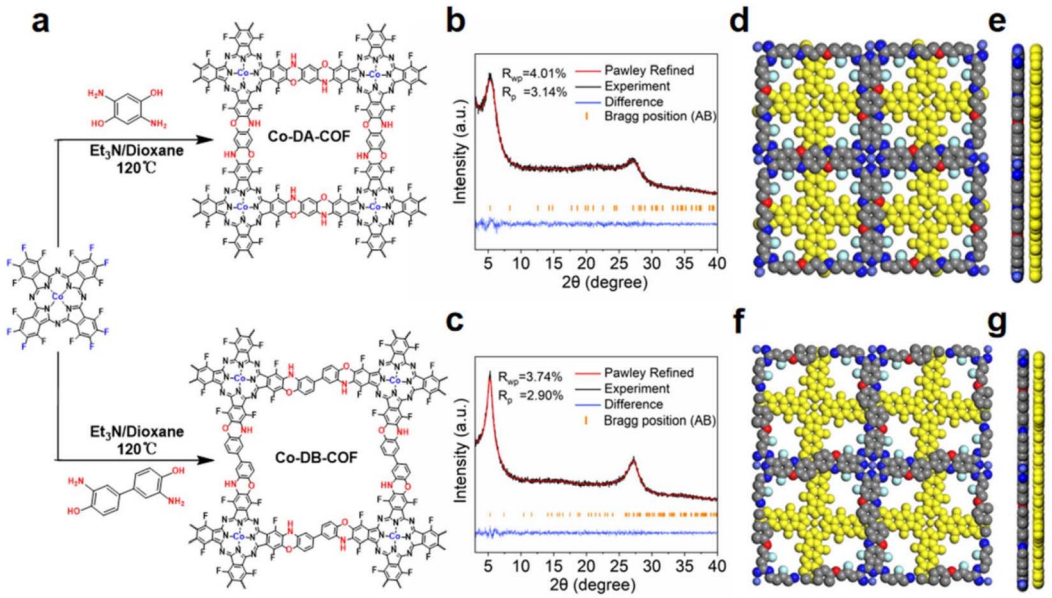

Fig. 21 (a) Synthetic route COFs. PXRD pattern of (b) Co-DA-COF and (c) Co-DB-COF. Simulated AB stacking models of Co-DA-COF (d and e) and Co-DB-COF (f and g). Reprinted with permission from ref. 59. Copyright 2025 The Royal Society of Chemistry.

carbon dioxide reduction reactions, while systematically outlining the effects of linker length, linker substituents, central metal, material morphology, and material dimensionality on the catalytic performance. Despite great progress that have been achieved, several challenges in the research of Pc-COFs should be fully addressed.

5.1 Strategies for improving electrical conductivity

Enhancing the conductivity of COF materials is a crucial strategy for improving electrocatalytic CO_2 reduction activity. Key approaches include: (i) Constructing extended conjugated systems by designing planar building units with large π-systems and facilitating long-range ordered π–π stacking to enhance electron cloud overlap, narrow the band gap, and promote charge carrier migration, thereby creating efficient "electron highways".[8] (ii) Introducing redox-active units or doping to significantly increase charge carrier concentration *via* chemical or electrochemical methods. Compositing with highly conductive materials such as carbon materials or conductive polymers to establish rapid electron transport networks.[17] (iii) Post-synthetic modification through chemical functionalization to adjust HOMO/LUMO energy levels and modulate the band gap

and conductivity.[29] (iv) Optimizing crystallinity and stacking mode by refining synthesis conditions to achieve highly crystalline COFs with reduced interlayer distances, strengthening π-orbital overlap and enhancing interlayer electron hopping.

5.2 Strategies for increasing active sites

Increasing the number of active sites is another crucial approach for enhancing the photoelectrocatalytic activity of COF catalysts. Key strategies encompass: (i) Structural design and precision synthesis constructing three-dimensional network structures. Compared to 2D COFs, 3D COFs effectively reduce interlayer stacking, providing more accessible pores and surfaces, thereby significantly increasing the density of exposed active sites.[99] (ii) Introducing sterically hindered substituents: incorporating bulky side groups or pillars between the layers of 2D COFs increases the interlayer spacing, preventing active centers from being obscured by dense π–π stacking and making them more accessible to reactants. (iii) Precise selection and synergistic utilization of metal centers. Selecting highly intrinsically active metal centers and dispersing them atomically within the COF framework to achieve extremely high atom utilization. (iv) Incorporating two or more different metal centers into the COF framework to synergistically modulate the adsorption energy of intermediates through electronic or geometric effects,[45] thereby enhancing the intrinsic activity of individual sites. The proportions of the linker and central metal are shown in Fig. 22. Post-synthetic modification and composite strategies. Anchoring additional metal ions or clusters onto pre-synthesized COFs through post-synthetic treatments to create new highly active sites.[112]

5.3 Strategies for enhancing framework stability

To enhance the stability of phthalocyanine-based COF materials under electrocatalytic and photocatalytic conditions, particular attention must be paid to their failure mechanisms in harsh environments such as electric fields, light exposure, electrolytes, and reactive intermediates. Effectively addressing issues including chemical degradation, deactivation of active sites, metal leaching, structural collapse, and insufficient electrical conductivity is essential. Key strategies involve: (i) employing highly stable irreversible linkage bonds or performing post-synthetic modifications on unstable bonds; (ii) forming composites with conductive carbon materials, such as *in situ* growth of Pc-COFs on substrates like graphene oxide, carbon nanotubes, or carbon fiber;[16] (iii) designing Pc-COFs with three-dimensional topological structures to effectively resist electrolyte penetration and internal stress induced by gas products; (iv) optimizing synthesis conditions (*e.g.*, solvent, temperature, catalyst) to obtain COFs with high crystallinity and low defect density.

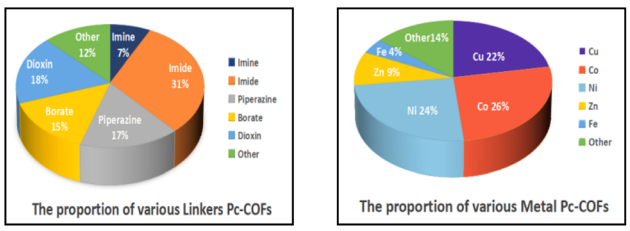

Fig. 22 The proportion of various linker and metal Pc-COFs (other: Nb, Ce, and H).

5.4 Deeper investigation into the mechanism

The elucidation of reaction mechanisms in Pc-COFs under either electrocatalytic or photocatalytic conditions represents a frontier and complex research topic. A clear revelation of these mechanisms requires the establishment of a multi-dimensional and multi-tiered research framework. Although significant progress has been made in the study of these reaction mechanisms, several challenges remain that require further investigation. For instance, the active sites in Pc-COFs constitute a complex system: whether the catalytic activity originates from the extended π-system of the phthalocyanine macrocycle, the central metal ions (*e.g.*, Co, Fe), their axial coordination sites, or other functional groups within the COF framework remains unclear. During catalytic processes, these sites may function synergistically, making it difficult to isolate and study individual contributions. Additionally, the detection and identification of reaction intermediates pose considerable challenges, as these species are often extremely short-lived, present in low concentrations, and highly reactive, particularly at solid–liquid interfaces. Furthermore, theoretical calculations, such as density functional theory (DFT), often employ idealized, finite periodic models that fail to account for structural defects, edge effects, disorder, and solvent interactions prevalent in practical materials, highlighting inherent limitations in current computational approaches. Consequently, more in-depth research by the scientific community is imperative to address these unresolved issues.

5.5 Large-scale synthesis and processing forming

In addition to the synthesis strategies and mechanism of COFs, the large-scale synthesis and processing forming of COFs materials are also key issues that need to be focused on. On one hand, the current synthesis of high-quality crystalline COFs mainly adopts the solvothermal method, which usually has a small scale and high cost. Developing efficient, low-cost, and scalable synthesis methods is the key to industrial application. On the other hand, most COFs are microcrystalline powders and are difficult to be processed into the films, fibers, or block materials required for devices. Improving their processability is an important research direction.

For further development, more attention will be paid to enriching the structure diversity of Pc-COFs and their performance enhancement in electrocatalytic and photocatalytic CO_2 reduction. We sincerely hope that this review will offer some helpful ideas to the researchers who focus on the basic principles for the design and preparation of COFs based on Pc-based monomers.

Author contributions

Li Yingying is responsible for writing, revising and submitting the thesis. Song Haiyan is in charge of collecting and organizing the literature materials. Zhu Wenbo contributed to drawing the relevant pictures in the article. Shuai Chao organized the references.

Conflicts of interest

The authors declare no conflicts of interest.

Data availability

Data sharing is not applicable to this article as no new data were created or analyzed in this study.

Acknowledgements

Financial support from the Gansu Province Higher Education Support Program for Young Doctor [grant number: 2023QB-16]. Qingyang Science and Technology Bureau Project [grant number: QY-STK-2024A-062]. Wuxi Jinjie Zhongsheng Biotechnology Co., Ltd. and Longdong University cooperation project [grant number: HXZK2479].

References

1 B. Yasemin, C. Rifat, E. Matem, C. Ozkaya, Y. Acikbas, N. Kabay and Y. GÖk, *Synth. Methods*, 2021, **280**, 116870, DOI: 10.1016/j.synthmet.2021.116870.
2 L. Barhoumi, A. Barake, N. M. Nooredeen, M. B. Ali, M. N. Abbas, J. Bausells and A. Errachid, *Electroanalysis*, 2017, **29**, 1586–1595, DOI: 10.1002/elan.201700005.
3 D. Gounden, N. Nombona and W. E. V. Zyl, *Coord. Chem. Rev.*, 2020, **420**, 213359, DOI: 10.1016/j.ccr.2020.213359.
4 W. Lee, S. B. Yuk, J. Choi, D. H. Jung, S. Choi, J. Park and J. P. Kim, *Dyes Pigm.*, 2012, **92**, 942–948, DOI: 10.1016/j.dyepig.2011.08.001.
5 M. Xu, L. D. Zheng, P. Wang, S. Wang, L. Xie and Y. Hua, *ACS Sustainable Chem. Eng.*, 2024, **12**, 18382–18389, DOI: 10.1021/acssuschemeng.4c07524.
6 P. Grishma, P. Jalaja, S. Satyam and P. K Jha, *Int. J. Energy Res.*, 2022, **46**, 15127–15142, DOI: 10.1002/er.8211.
7 L. Xie, Y. Wang, Q. Kong and R. Cao, *ChemCatChem*, 2024, **16**, e202400956, DOI: 10.1002/cctc.202400956.
8 J. Feng, Q. Hu, X. Yue, Q. Chen, C. Gao, J. Gu, L. Zhang, L. Zhang, H. Dai, F. Yang, G. Lin, K. Ping and Z. Xu, *Appl. Catal., B*, 2025, **366**, 125027, DOI: 10.1016/j.apcatb.2025.125027.
9 Y. Gök, S. Donmez, R. Erdem and H. Z. Gök, *ChemPlusChem*, 2025, **90**, e202500207, DOI: 10.1002/cplu.202500207.
10 P. Kichambare, S. Rodrigues, D. Firsich, W. A. Feld, K. Hankins, P. B. Balbuena and L. Scanlon, *Chem. Phys. Lett.*, 2024, **841**, 141179, DOI: 10.1016/j.cplett.2024.141179.
11 H. Pan, Y. Ren, Q. Wang, J. Hu, Y. Zhang, K. Wang and J. Jiang, *Coord. Chem. Rev.*, 2025, **527**, 216404, DOI: 10.1016/j.ccr.2024.216404.
12 Y. Zhao, J. Xu, Z. Huang, Y. Wang, Y. Li and H. Wei, *ACS Appl. Mater. Interfaces*, 2025, **17**, 12156–12168, DOI: 10.1021/acsami.4c20810.
13 M. Xu, K. Chen, L. Zhu, S. Zhang, M. Wang, L. He, Z. Zhang and M. Du, *Langmuir*, 2021, **37**, 13479–13492, DOI: 10.1021/acs.langmuir.1c02253.
14 L. Hui, X. Ding and B. Han, *Chem. - Eur. J.*, 2016, **22**, 11863–11868, DOI: 10.1002/chem.201602337.
15 R. Jiang, X. Wang, C. Shi, Y. Li, Q. Xu, X. Yang, C. Li, C. Liu, Z. Liu, K. Wang, J. Jiang and Y. Feng, *ACS Appl. Mater. Interfaces*, 2025, **17**, 24005–24013, DOI: 10.1021/acsami.5c02534.
16 M. Wang, L. Zhu, S. Zhang, Y. Lou, S. Zhao, Q. Tan, L. He and M. Du, *Sens. Actuators, B*, 2021, **338**, 129826, DOI: 10.1016/j.snb.2021.129826.
17 N. Li, H. Gao, Z. Liu, Q. Zhi, B. Li, L. Gong, B. Chen, T. Yang, K. Wang, P. Jin and J. Jiang, *Sci. China: Chem.*, 2023, **66**, 1417–1424, DOI: 10.1007/s11426-023-1524-4.
18 L. Wang, G. Huang, L. Zhang, R. Lian, J. Huang, H. She, C. Liu and Q. Wang, *J. Energy Chem.*, 2022, **64**, 85–92, DOI: 10.1016/j.jechem.2021.04.053.
19 M. Chen, H. Li, C. Liu, J. Liu, Y. Feng, A. G. H. Wee and B. Zhang, *Coord. Chem. Rev.*, 2021, **435**, 213778, DOI: 10.1016/j.ccr.2021.213778.
20 S. Huang, K. Chen and T. Li, *Coord. Chem. Rev.*, 2022, **464**, 214563, DOI: 10.1016/j.ccr.2022.214563.
21 O. V. Kharissova, Y. P. Méndez, B. I. Kharisov, A. L. Nikolaev, E. L. olito and L. T. Gonzalez, *Particuology*, 2024, **90**, 236–265, DOI: 10.1016/j.partic.2023.12.008.
22 H. Q. Pham, D. Q. Le, N. Pham-Tran, Y. Kawazoe and D. Nguyen-Manh, *RSC Adv.*, 2019, 29440–29447, DOI: 10.1039/C9RA05159G.
23 L. Chen, K. Furukawa, J. Gao, A. Nagai, T. Nakamura, Y. Dong and D. Jiang, *J. Am. Chem. Soc.*, 2014, **136**, 9806–9809, DOI: 10.1021/ja502692w.
24 X. Wang, Y. Jin, N. Li, H. Zhang, X. Liu, X. Yang, H. Pan, T. Wang, K. Wang, D. Qi and J. Jiang, *Angew. Chem., Int. Ed.*, 2024, **63**, e202401014, DOI: 10.1002/anie.202401014.
25 X. Wang, M. Bahri, Z. Fu, M. A. Little, L. Liu, H. Niu, N. D. Browning, S. Y. Chong, L. Chen, J. W. Ward and A. I. Cooper, *J. Am. Chem. Soc.*, 2021, **143**, 15011–15016, DOI: 10.1021/jacs.1c08351.
26 X. Ding, L. Chen, Y. Honsho, X. Feng, O. Saengsawang, J. Guo, A. Saeki, S. Seki, S. Irle, S. Nagase, V. Parasuk and D. Jiang, *J. Am. Chem. Soc.*, 2011, **133**, 14510–14513, DOI: 10.1021/ja2052396.
27 Y. Yue, P. Cai, K. Xu, H. Li, H. Chen, H. Zhou and N. Huang, *J. Am. Chem. Soc.*, 2021, **143**, 18052–18060, DOI: 10.1021/jacs.1c06238.
28 X. Guan, Q. Fang, Y. Yan and S. Qiu, *Acc. Chem. Res.*, 2022, **55**, 1912–1927, DOI: 10.1021/acs.accounts.2c00200.
29 B. Han, B. Liang, E. Zhang, J. Li, Y. Li, Q. Zhang, Z. Xie, H. Wang and J. Jiang, *Adv. Funct. Mater.*, 2024, **34**, 2404289, DOI: 10.1002/adfm.202404289.

30 X. Liu, C. Guan, S. Ding, W. Wang, H. Yan, D. Wang and L. Wan, *J. Am. Chem. Soc.*, 2013, **135**, 10470–10474, DOI: 10.1021/ja403464h.
31 A. C. Marele, R. Mas-Balleste, L. Terracciano, J. Rodríguez-Fernández, I. Berlanga, S. S. Alexandre, R. Otero, J. M. Gallego, F. Zamora and J. M. Gómez-Rodríguez, *Chem. Commun.*, 2012, **48**, 6779–6781, DOI: 10.1039/c2cc32270f.
32 M. O. Blunt, J. C. Russell, N. R. Champness and P. H. Beton, *Chem. Commun.*, 2010, **46**, 7157–7159, DOI: 10.1039/c0cc01810d.
33 R. Gutzler, H. Walch, G. Eder, W. M. Hecklab and M. Lackinger, *Chem. Commun.*, 2009, **45**, 4456–4458, DOI: 10.1039/b906836h.
34 B. P. Biswal, S. Chandra, S. Kandambeth, B. Lukose, T. Heine and R. Banerjee, *J. Am. Chem. Soc.*, 2013, **135**, 5328–5331, DOI: 10.1021/ja4017842.
35 N. L. Campbell, R. Clowes and L. K. Ritchie, *Chem. Mater.*, 2009, **21**, 204–206, DOI: 10.1021/cm802981m.
36 B. J. Smith and W. R. Dichtel, *J. Am. Chem. Soc.*, 2014, **136**, 8783–8789, DOI: 10.1021/ja5037868.
37 A. P. Côté, A. I. Benin, N. W. Ockwig, M. O'Keeffe, A. J. Matzger and O. M. Yaghi, *Science*, 2005, **310**, 1166–1170, DOI: 10.1126/science.1120411.
38 M. A. A. Musa, C. Yin and R. M. Savory, *Mater. Chem. Phys.*, 2010, **123**, 5–8, DOI: 10.1016/j.matchemphys.2010.04.009.
39 M. Teng, J. Yuan, Y. Li, C. Shi, Z. Xu, C. Ma, L. Yang, C. Zhang, J. Gao and Y. Li, *J. Colloid Interface Sci.*, 2024, **654**, 348–355, DOI: 10.1016/j.jcis.2023.10.041.
40 Y. Song, Y. Meng, K. Chen, G. Huang, S. Li and L. Hu, *Bioelectrochemistry*, 2024, **156**, 108630, DOI: 10.1016/j.bioelechem.2023.108630.
41 R. Li, T. Yang, J. Zhang, Z. Xu and S. Chao, *Int. J. Hydrogen Energy*, 2025, **98**, 648–656, DOI: 10.1016/j.ijhydene.2024.12.100.
42 X. Tian, X. Huang, J. Shi, J. Zhou, C. Guo, R. Wang, Y. Wang, M. Lu, Q. Li, Y. Chen, S. Li and Y. Lan, *CCS Chem.*, 2023, **5**, 2557–2566, DOI: 10.31635/ccschem.022.202202519.
43 R. Jiang, Q. Zhi, B. Han, N. Li, K. Wang, D. Qi, W. Li and J. Jiang, *Chem. Eng. J.*, 2024, **489**, 151232, DOI: 10.1016/j.cej.2024.151232.
44 J. Yuan, S. Chen, Y. Zhang, R. Li, J. Zhang and T. Peng, *Adv. Mater.*, 2022, **34**, 2203139, DOI: 10.1002/adma.202203139.
45 M. Zhang, J. Liao, R. Li, S. Sun, M. Lu, L. Dong, P. Huang, S. Li, Y. Cai and Y. Lan, *Natl. Sci. Rev.*, 2023, **10**, nwad226, DOI: 10.1093/nsr/nwad226.
46 D. Er, L. Dong and V. B. Shenoy, *J. Phys. Chem. C*, 2016, **120**, 174–178, DOI: 10.1021/acs.jpcc.5b11928.
47 Z. Meng, R. M. Stolz and K. A. Mirica, *J. Am. Chem. Soc.*, 2019, **141**, 11929–11937, DOI: 10.1021/jacs.9b03441.
48 M. Zhang, D. Si, J. Yi, S. Zhao, Y. Huang and R. Cao, *Small*, 2020, **16**, e200525, DOI: 10.1002/smll.202005254.
49 H. Zhong, M. Wang, M. Ghorbani-Asl, J. Zhang, K. Ly, Z. Liao, Gu. Chen, Y. Wei, B. P. Biswal, E. Zschech, I. M. Weidinger, A. V. Krasheninnikov, R. Dong and X. Feng, *J. Am. Chem. Soc.*, 2021, **143**, 19992–20000, DOI: 10.1021/jacs.1c11158.
50 C. Yao, J. Li, W. Gao and Q. Jiang, *Chem.–Eur. J.*, 2018, **24**, 11051–11058, DOI: 10.1002/chem.201800363.
51 V. Neti, X. Wu, S. Deng and L. Echegoyen, *CrystEngComm*, 2013, **15**, 6892–6895, DOI: 10.1039/c3ce40706c.
52 S. Jin, M. Supur, M. Addicoat, K. Furukawa, L. Chen, T. Nakamura, S. Fukuzumi, S. Irle and D. Jiang, *J. Am. Chem. Soc.*, 2015, **137**, 7817–7827, DOI: 10.1021/jacs.5b03553.
53 E. L. Spitler, J. W. Colson, F. J. Uribe-Romo, A. R. Woll, M. R. Giovino, A. Saldivar and W. R. Dichtel, *Angew. Chem.*, 2012, **124**, 2677–2681, DOI: 10.1002/ange.201107070.
54 E. L. Spitler and W. R. Dichtel, *Nat. Chem.*, 2010, **2**, 672–677, DOI: 10.1038/NCHEM.695.
55 M. Liu, N. Li, S. Cao, X. Wang, X. Lu, L. Kong, Y. Xu and X. Bu, *Adv. Mater.*, 2022, **34**, 2107421, DOI: 10.1002/adma.202107421.
56 J. Campos, *Nat. Rev. Chem.*, 2020, **4**, 696–702, DOI: 10.1038/s41570-020-00226-5.
57 X. Chen, M. Zeng, J. Yang, N. Hu, X. Duan, W. Cai, Y. Su and Z. Yang, *Nanomaterials*, 2023, **13**, 1660, DOI: 10.3390/nano13101660.
58 M. Wang, S. Fu, P. Petkov, Y. Fu, Z. Zhang, Y. Liu, J. Ma, G. Chen, S. M. Gali, L. Gao, Y. Lu, S. Paasch, H. Zhong, H. Steinrück, E. Cánovas, E. Brunner, D. Beljonne, M. Bonn, H. I. Wang, R. Dong and X. Feng, *Nat. Mater.*, 2023, **22**, 880–887, DOI: 10.1038/s41563-023-01581-6.
59 F. Lin, W. Lin, J. Lin, Y. Hui, J. Chenace and Y. Wang, *J. Mater. Chem. A*, 2025, **13**, 3287–3294, DOI: 10.1039/d4ta07561g.
60 D. Jiang, Y. Li, S. Wu, L. Lan and J. Liu, *Microchim. Acta*, 2025, **192**, 251, DOI: 10.1007/s00604-025-07105-0.
61 Q. Zhang, Z. Zhu, L. Liu, H. Huang, X. Chen, Y. Bian, M. Shao, X. Wei, C. Wang, D. Wang, J. Dong, Y. Guo, Y. Zhu and Y. Liu, *Angew. Chem., Int. Ed.*, 2024, **63**, e202319027, DOI: 10.1002/anie.202319027.
62 J. Zhao, M. Zhou, J. Chen, L. Tao, Q. Zhang, Z. Li, S. Zhong, H. Fu, H. Wang and L. Wu, *Chem. Eng. J.*, 2021, **425**, 131630, DOI: 10.1016/j.cej.2021.131630.
63 Z. Wu, X. Zhang, P. Yang, Z. Niu, F. Gao, Y. Zhang, L. Chi, S. Sun, J. DuanMu, P. Lu, Y. Li and M. Gao, *J. Am. Chem. Soc.*, 2023, **145**, 24338–24348, DOI: 10.1021/jacs.3c09255.
64 L. Huang, Z. Liu, G. Gao, C. Chen, Y. Xue, J. Zhao, Q. Lei, M. Jin, C. Zhu, Y. Han, J. S. Francisco and X. Lu, *J. Am. Chem. Soc.*, 2023, **145**, 26444–26451, DOI: 10.1021/jacs.3c10600.
65 X. Yang, X. Li and Y. Huang, *Front. Chem. Sci. Eng.*, 2024, **18**, 79, DOI: 10.1007/s11705-024-2434-0.
66 Q. Zhi, R. Jiang, X. Yang, Y. Jin, D. Qi, K. Wang, Y. Liu and J. Jiang, *Nat. Commun.*, 2024, **15**, 678, DOI: 10.1038/s41467-024-44899-8.
67 Y. Gong, J. Mei, W. Shi, J. Liu, D. Zhong and T. Lu, *Angew. Chem.*, 2024, **136**, e202318735, DOI: 10.1002/ange.202318735.
68 M. Lu, M. Zhang, C. Liu, J. Liu, L. Shang, M. Wang, J. Chang, S. Li and Y. Lan, *Angew. Chem.*, 2021, **60**, 4864–4871, DOI: 10.1002/anie.202011722.

69 J. Yu, Y. Wang and Y. Li, *Phys. Chem. Chem. Phys.*, 2024, **26**, 15120, DOI: 10.1039/d4cp01257g.
70 Y. Rong, T. Liu, J. Sang, R. Li, P. Wei, H. Li, A. Dong, L. Che, Q. Fu, D. Gao and G. Wang, *Angew. Chem.*, 2023, **62**, e202309893, DOI: 10.1002/anie.202309893.
71 J. Li, Y. Chen, B. Yao, W. Yang, X. Cui, H. Liu, S. Dai, S. Xi, Z. Sun, W. Chen, Y. Qin, J. Wang, Q. He, C. Ling, D. Wang and Z. Zhang, *J. Am. Chem. Soc.*, 2024, **146**, 5693–5701, DOI: 10.1021/jacs.4c00475.
72 Q. Yang, Y. Chen, N. Liu, S. Li, M. Chen, W. Zheng, Y. Fu, J. Han, R. D. Rodriguez, Y. Hou and T. Zhang, *J. Am. Chem. Soc.*, 2025, **147**, 22132–22140, DOI: 10.1021/jacs.5c06660.
73 X. Yang, Y. Jin, B. Yu, L. Gong, W. Liu, X. Liu, X. Chen, K. Wang and J. Jiang, *Sci. China: Chem.*, 2022, **65**, 1291–1298, DOI: 10.1007/s11426-022-1269-0.
74 H. Wu, M. Zeng, X. Zhu, C. Tian, B. Mei, Y. Song, X. Du, Z. Jiang, L. He, C. Xia and S. Dai, *ChemElectroChem*, 2018, **5**, 2717–2721, DOI: 10.1002/celc.201800806.
75 X. Liu, A. Zhang, R. Ma, B. Wu, T. Wen, Y. Ai, M. Sun, J. Jin, S. Wang and X. Wang, *Chin. Chem. Lett.*, 2022, **33**, 3549–3555, DOI: 10.1016/j.cclet.2022.03.001.
76 X. Yang, L. Gong, K. Wang, S. Ma, W. Liu, B. Li, N. Li, H. Pan, X. Chen, H. Wang, J. Liu and J. Jiang, *Adv. Mater.*, 2022, **34**, 2207245, DOI: 10.1002/adma.202207245.
77 K. S. Song, P. W. Fritz, D. F. Abbott, L. N. Poon, C. M. Caridade, F. Gándara, V. Mougel and A. Coskun, *Angew. Chem., Int. Ed.*, 2023, **62**, e202309775, DOI: 10.1002/anie.202309775.
78 Z. Chen, N. Li and Q. Zhang, *Small Struct.*, 2024, **5**, 2300495, DOI: 10.1002/sstr.202300495.
79 S. Chen, L. Chen, L. Zhang and X. Li, *Sep. Purif. Technol.*, 2025, **353**, 12862, DOI: 10.1016/j.seppur.2024.128623.
80 J. Wang, W. Zhang, H. Chen, Q. Ding, J. Xua, Q. Yua, M. Fang and L. Zhang, *J. Chromatogr. A*, 2023, **1692**, 463847, DOI: 10.1016/j.chroma.2023.463847.
81 P. D. Harvey, *J. Porphyrins Phthalocyanines*, 2023, **27**, 1015–1027, DOI: 10.1142/S1088424623300112.
82 X. Song, F. Zhou, M. Yao, C. Hao and J. Qiu, *ACS Sustainable Chem. Eng.*, 2020, **8**, 10185–10192, DOI: 10.1021/acssuschemeng.0c02563.
83 Y. Yue, P. Cai, X. Xu, H. Li, H. Chen, H. Zhou and N. Huang, *Angew. Chem., Int. Ed.*, 2021, **60**, 10806–10813, DOI: 10.1002/ange.202100717.
84 R. Jiang, C. Li, Q. Xu, Z. Liu, X. Yang, C. Li, Q. Xu, X. Zhan, K. Wang, L. Zhang, J. Jiang and Y. Feng, *Small*, 2025, **21**, 2410405, DOI: 10.1002/smll.202410405.
85 X. Yang, D. Si, H. Li, R. Cao and Y. Huang, *Mater. Chem. Front.*, 2024, **8**, 1611, DOI: 10.1039/d3qm01190a.
86 M. Zhang, J. Huang, C. Liang, X. Chen and P. Liao, *J. Am. Chem. Soc.*, 2024, **146**, 31034–31041, DOI: 10.1021/jacs.4c10675.
87 A. Kumar, M. Ubaidullah, B. Pandit, G. Yasin, R. K. Gupta and G. Zhang, *Discover Nano*, 2023, **18**, 109, DOI: 10.1186/s11671-023-03890-w.
88 X. Zhan, Y. Jin, B. Han, Z. Zhou, B. Chen, X. Ding, F. Li, Z. Suo, R. Jiang, D. Qi, K. Wang and J. Jiang, *Chin. J. Catal.*, 2025, **69**, 271–281, DOI: 10.1016/S1872-2067(24)60196-8.
89 S. Rajappa, P. G. Shivarathri, M. H. Rajappa, M. C. Devendrachari and H. M. N. Kotresh, *Polyhedron*, 2024, **252**, 116881, DOI: 10.1016/j.poly.2024.116881.
90 Y. Jin, Q. Zhi, H. Wang, X. Zhan, D. Qi, B. Yu, X. Ding, T. Wang, H. Liu, M. Tang, J. Liu and J. Jiang, *Natl. Sci. Rev.*, 2025, **1**, nwae396, DOI: 10.1093/nsr/nwae396.
91 D. Shindell, D. Shindell and C. J. Smith, *Nature*, 2019, **573**, 408–411, DOI: 10.1038/s41586-019-1554-z.
92 Q. Yi, W. Li, J. Feng and K. Xie, *Chem. Soc. Rev.*, 2015, **44**, 5409–5445, DOI: 10.1039/c4cs00453a.
93 S. J. Davis, K. Caldeira and H. D. Matthews, *Science*, 2010, **329**, 1330–1333, DOI: 10.1126/science.1188566.
94 Y. Liao, *E3S Web Conf.*, 2024, **553**, 1005, DOI: 10.1051/e3sconf/202455301005.
95 H. Wang, X. Wang, Y. Jiang, M. Li, H. Peng, G. Ma, L. Zhu, I. Shakir and Y. Xu, *Chem. Rec.*, 2025, **25**, e202400244, DOI: 10.1002/tcr.202400244.
96 M. Li, B. Han, S. Li, Q. Zhang, E. Zhang, L. Gong, D. Qi, K. Wang and J. Jiang, *Small*, 2024, **20**, 2310147, DOI: 10.1002/smll.202310147.
97 B. Han, Y. Jin, B. Chen, W. Zhou, B. Yu, C. Wei, H. Wang, K. Wang, Y. Chen, B. Chen and J. Jiang, *Angew. Chem., Int. Ed.*, 2022, **61**, e202114244, DOI: 10.1002/anie.202114244.
98 B. Han, X. Ding, B. Yu, H. Wu, W. Zhou, W. Liu, C. Wei, B. Chen, D. Qi, H. Wang, K. Wang, Y. Chen, B. Chen and J. Jiang, *J. Am. Chem. Soc.*, 2021, **143**, 7104–7113, DOI: 10.1021/jacs.1c02145.
99 Q. Zhang, B. Han, Y. Jin, M. Li, E. Zhang and J. Jiang, *Chin. Chem. Lett.*, 2024, **36**, 110330, DOI: 10.1016/j.cclet.2024.110330.
100 T. Xie, S. Chen, Y. Yue, T. Sheng, N. Huang and Y. Xiong, *Angew. Chem., Int. Ed.*, 2024, **63**, e202411188, DOI: 10.1002/anie.202411188.
101 M. Lu, M. Zhang, C. Liu, J. Liu, L. Shang, M. Wang, J. Chang, S. Li and Y. Lan, *Angew. Chem.*, 2021, **133**, 4914–4921, DOI: 10.1002/ange.202011722.
102 N. Huang, K. H. Lee, Y. Yue, X. Xu, S. Irle, Q. Jiang and D. Jiang, *Angew. Chem., Int. Ed.*, 2020, **59**, 16587–16593, DOI: 10.1002/ange.202005274.
103 M. Abdinejad, C. Dao, X. Zhang and H. B. Kraatz, *J. Energy Chem.*, 2021, **58**, 162–169, DOI: 10.1016/j.jechem.2020.09.039.
104 J. X. Xuan, K. Jiang, S. Huang, B. Feng, F. Qiu, S. Han, J. Zhu and X. Zhuang, *Mater. Sci.*, 2022, **57**, 10129–10140, DOI: 10.1007/s10853-022-07303-8.
105 C. S. Diercks, Y. Liu, K. E. Cordova and O. M. Yaghi, *Nat. Mater.*, 2018, **17**, 301–307, DOI: 10.1038/s41563-018-0033-5.
106 W. Lin, F. Lin, J. Lin, Z. Xiao, D. Yuan and Y. Wang, *J. Am. Chem. Soc.*, 2024, **146**, 16229–16236, DOI: 10.1021/jacs.4c04185.
107 X. Dong, Y. Si, Q. Wang, S. Wang and S. Zang, *Adv. Mater.*, 2021, **33**, 2101568, DOI: 10.1002/adma.202101568.
108 S. Roy and E. Reisner, *Angew. Chem.*, 2019, **131**, 12308–12312, DOI: 10.1002/anie.201907082.

109 X. Lu, X. Fang, Y. Jin, H. Wang, X. Li, Y. Xie and J. Jiang, *Chem. Eng. J.*, 2025, **508**, 161018, DOI: 10.1016/j.cej.2025.161018.
110 Y. Zhang, L. Zang, S. Zhao, W. Cheng, L. Zhang and L. Sun, *J. Colloid Interface Sci.*, 2024, **655**, 1–11, DOI: 10.1016/j.jcis.2023.10.111.
111 Y. Zhang, X. Guan, Z. Meng and H. Jiang, *J. Am. Chem. Soc.*, 2025, **147**, 3776–3785, DOI: 10.1021/jacs.4c16538.
112 C. Luo, Y. Zhou, Y. Guo, X. Li, R. Li and T. Peng, *ACS Sustainable Chem. Eng.*, 2024, **12**, 18691–18703, DOI: 10.1021/acssuschemeng.4c08044.